

Inherited structural controls on fault geometry, architecture and hydrothermal activity: an example from Grimsel Pass, Switzerland

Thomas M. Belgrano¹ · Marco Herwegen¹ · Alfons Berger¹

Received: 26 October 2015 / Accepted: 17 March 2016 / Published online: 6 April 2016
© Swiss Geological Society 2016

Abstract Exhumed faults hosting hydrothermal systems provide direct insight into relationships between faulting and fluid flow, which in turn are valuable for making hydrogeological predictions in blind settings. The Grimsel Breccia Fault (Aar massif, Central Swiss Alps) is a late Neogene, exhumed dextral strike-slip fault with a maximum displacement of 25–45 m, and is associated with both fossil and active hydrothermal circulation. We mapped the fault system and modelled it in three dimensions, using the distinctive hydrothermal mineralisation as well as active thermal fluid discharge (the highest elevation documented in the Alps) to reveal the structural controls on fluid pathway extent and morphology. With progressive uplift and cooling, brittle deformation inherited the mylonitic shear zone network at Grimsel Pass; preconditioning fault geometry into segmented brittle reactivations of ductile shear zones and brittle inter-shear zone linkages. We describe ‘pipe’-like, vertically oriented fluid pathways: (1) within brittle fault linkage zones and (2) through along-strike-restricted segments of formerly ductile shear zones reactivated by brittle deformation. In both cases, low-permeability mylonitic shear zones that escaped brittle reactivation provide important hydraulic seals. These observations show that fluid flow along brittle fault planes is not planar, but rather highly channelised into sub-vertical flow domains, with important implications for the exploration and exploitation of geothermal energy.

Keywords Fluid pathways · Structure · Crystalline basement · Geothermal · Brittle deformation · Structural inheritance

1 Introduction

A hydrogeological fluid pathway is comprised of a continuously permeable zone surrounded by a zone of relative lower permeability, where the extent and arrangement of these zones define the pathways hydraulic architecture (Caine et al. 1996). Along fault-related fluid pathways, fault architecture is the dominant control on permeability structure, and therefore, fluid flow localisation (Evans et al. 1997). However, modern fault-zone investigations recognise inherent heterogeneity of these architectures in natural examples, and strive to delineate order through paired structural and hydrological consideration (Faulkner et al. 2010). Previous studies demonstrate that fluid flow in fault-zones is locally influenced by structural complexities, and consequently can be anisotropic, directional, dynamic (Sibson 1996; Schulz and Evans 2000; Kirkpatrick et al. 2008; Cox et al. 2001; Eichhubl et al. 2009; Walker et al. 2012) and channelised (Barton et al. 1995; Annunziatellis et al. 2008; Dockrill and Shipton 2010; Burnside et al. 2013). Analyses of proxies for flow in fossil systems reveal that enhanced fluid flux along these channels is commonly associated with complexities in fault geometry: step-overs, linkages, intersections, releasing bends and dilational jogs (Sibson 1996; Perello et al. 2001; Micklethwaite et al. 2015).

Current understanding of fault systems is established on the holistic consideration of a collection of individually recognised relationships in nature: mechanical anisotropy and fault initiation (Crider 2015); fault geometry and damage-zone architecture (Sibson 1985; Caine et al. 1996;

Editorial handling: S. Schmid.

✉ Thomas M. Belgrano
thomas.belgrano@geo.unibe.ch

¹ Institute of Geological Sciences, University of Bern,
Baltzerstrasse 3, 3012 Bern, Switzerland

Micklethwaite et al. 2015); fracture networks and mineralisation (Sibson 1996; Tripp and Vearncombe 2004). However, direct observation of natural examples of these relationships operating in unison within a single system are rare (Moir et al. 2013; Soden et al. 2014), but serve to validate their multilateral interdependence (Faulkner et al. 2010).

To examine the interaction between pre-existing anisotropy, faulting, and fluid flow, we investigate an exhumed, formerly ductile strike-slip fault system hosting both fossil and active hydrothermal circulation at Grimsel Pass in the Central Swiss Alps. The fault, here termed the Grimsel Breccia Fault (GBF), has been well documented from a mineralogical and geochemical perspective (Hofmann et al. 2004). In this paper, we characterise the composition, structure and fluid flow system of the fault, closing the gap on the previously undescribed controls on its resident hydrothermal activity. We describe the structures and fluid pathways of the GBF at different scales, split over the following three sections: (1) A map and structural analysis of the fault, showing spatial relationships on the order of metres to kilometres between the fault, its damage zone, mineralisation, hydrothermal discharge and structural environment. (2) Line-intercept discontinuity analyses of the macroscopic fracture network and fault-zone features at the millimetre to metre scale. (3) Microstructural observations at the micrometre to millimetre scale. Finally, the results are considered in light of the inherited influences of pre-existing features, fluid-associated deformation processes and the resulting structurally controlled fluid pathways. When describing deformation at Grimsel Pass, strict terminology must be employed to differentiate between features formed by dominantly ductile or brittle processes. In order to specify features within the brittle fault system, we utilise the structural terms ‘fault’, ‘master fault’, ‘fault core’, ‘fault linkages’ and ‘damage zone’ (Fig. 1); whereas,

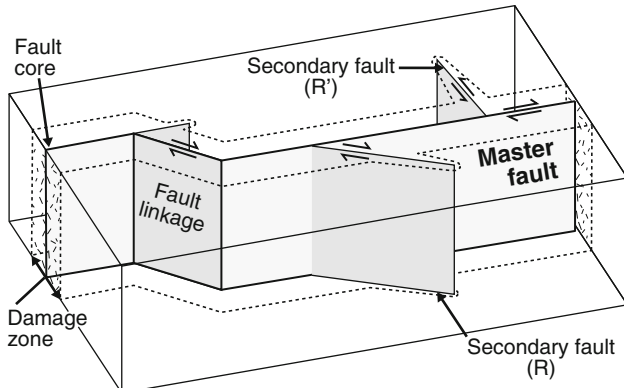


Fig. 1 Brittle fault terminology. Geometric and architectural terminologies schematically outlined in a simplified brittle fault system. “R” and “R’” refer to synthetic and antithetic Riedel orientations respectively

when referring to mylonitic shear zones formed by dominantly ductile processes, we use the term ‘shear zone’ (SZ).

2 Geological framework

The study area is centred on Grimsel Pass in the Aar massif, Central Swiss Alps (Fig. 2). The Aar massif is the largest External Crystalline Massif of the Swiss Alps, comprised of post-Variscan plutons intruded into pre-Variscan basement and Permocarboniferous sediments (Abrecht 1994). The GBF is hosted by the Southwestern Aar granite (SWAGr) and its country rock, the Grimsel Zone. The SWAGr has also been termed the Southern Aar granite (Schaltegger 1990), though is not to be confused with the separate Southern Aar granite east of the Reuss Valley (Schaltegger and Corfu 1992). The SWAGr, a calc-alkaline meta-granite, is the southernmost pluton of the Central Aar granite suite (Schaltegger 1990), which includes the Grimsel granodiorite (299 ± 2 Ma) and the Central Aar granite (297 ± 2 Ma) to the north (Schaltegger and Corfu 1992). Intrusion post-dates Variscan collision, so the plutons lack major pre-Alpine deformation structures. The Grimsel Zone is a strip of pervasively sheared gneisses 0.5–1 km wide, consisting of foliated pre-Variscan amphibolites, para- and orthogneisses and post-Variscan

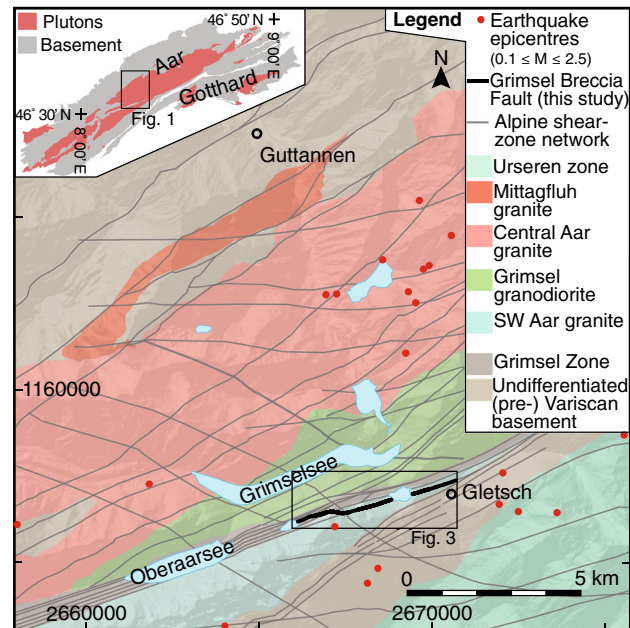


Fig. 2 Geological map of the Haslital, Aar Massif. Study area (box) and Grimsel Breccia Fault indicated. Lithologies after Stalder (1964) and Abrecht (1994); Alpine shear zone network after Baumberger (2015) and Wehrens (2015). Regional epicentres of earthquakes (magnitudes ranging from 0.1 to 2.5) recorded since 1971 (Swiss Seismological Service 2009; Deichmann et al. 2011, 2012; Diehl et al. 2013, 2014, 2015)

meta-volcanics (Stalder 1964; Oberhänsli et al. 1988). The basement rocks of the Aar massif, the protolith of the Grimsel Zone (Fig. 2), record deformational and metamorphic overprints from Proterozoic, Ordovician, Variscan and Alpine events (Stalder 1964; Steck 1966, 1968, 1984; Schaltegger 1993; Schaltegger et al. 2003). Consequently, these host rocks are structurally more complex and mechanically heterogeneous in comparison to the SWAGr.

The Alpine evolution of the study area can be summarised as follows (Steck 1966, 1968; Challandes et al. 2008; Rolland et al. 2009; Wehrens 2015): (1) Greenschist facies NNW-vergent thrusting during the compressional Handegg phase from 20–17 Ma. (2) Between 14–12 Ma, transpression caused dextral shearing during the Oberaar phase, exploiting oversteepened Handegg phase structures. (3) During steady exhumation of the Aar massif, retrograde deformation continued through the quartz ductile–brittle transition between 7 and 5 Ma (Wehrens 2015). (4) Brittle deformation was localised into discrete structures, marking the onset of predominantly cataclastic deformation along the GBF, and the beginning of this study's scope.

This polyphase Alpine deformation resulted in a complex 3D network of mylonitic SZs throughout the Aar massif (Fig. 2). Shear zones range from <1 cm to >100 m thick, and extend up to tens of km in length, their frequency being inversely correlated to SZ thickness (Baumberger 2015; Wehrens 2015). Subsequent embrittlement of these pre-existing SZs is reported throughout the Aar massif, manifesting as breccias, cataclasites and fault gouges (Keusen et al. 1989; Kralik et al. 1992; Rolland et al. 2009; Wehrens 2015). We group the prominent WSW-ENE striking SZs at Grimsel pass into the Grimsel Shear Zone set (Fig. 3: GSZ 1–4), which delimits NW–SE striking SZs that extend through the central Aar massif. The Southern Boundary Shear Zone (Fig. 3: SB SZ) separates the SWAGr from the Ausserberg-Avat Zone in the south of the study area.

High conductivity and distinctive, long-lived hydrothermal activity clearly differentiates the GBF and its formation mechanisms from the multitude of other brittle structures in the Aar massif. The fault breccias are associated with a rare example of epithermal-style mineralisation by topographically driven fluid flow (Hofmann et al. 2004). Mineralisation is of approximately Pliocene age, and consists of quartz (including microcrystalline varieties), adularia, hydrothermal clays, pyrite, marcasite, and molybdenite with significant but sub-economic enrichment in Mo, As, Sb, Au, Cs, Hg, Tl (Hofmann et al. 2004). Locally, microcrystalline quartz occurs both as chalcedony (length-fast; Hofmann et al. 2004) and quartzine (length-slow; Stalder 1964). For our purposes, these varieties are termed ‘microcrystalline quartz’ or ‘chert’ where forming sedimentary bands in pore space.

In addition to the mineralisation record, active sub-thermal waters of meteoric origin discharge from the GBF system at a spring in Gletsch (ca. 18 °C; Niggli 1965) and in a tunnel intersecting the fault (22–28.2 °C; Pfeifer et al. 1992; Hofmann et al. 2004). Current reservoir temperatures for the tunnel inflows are inferred to be at least 100 °C from their silica content, with estimates from 76° to 124° (Pfeifer et al. 1992), which with a present geothermal gradient of ca. 25 °C/km (Bodmer 1982) indicates a maximum circulation depth of 4 ± 1 km. The tunnel inflows are the highest documented hydrothermal discharge in the Alps (1908 m; Sonney and Vuataz 2008). Topographically driven circulation of thermal waters through fault systems in the Alps has been extensively documented from hydrothermal springs issuing from valley floors and valley-altitude tunnels (Vuataz 1982; Bianchetti et al. 1992; Rybach 1995; Perello et al. 2001; Baietto et al. 2009). However, the discharge at Grimsel Pass occurs at a topographic high, with negative relief to the valley floors on either side of the pass. In this context, Pfeifer et al. (1992) as well as Hofmann et al. (2004) recognised the requirement for a strongly focused fluid pathway to effectively seal the system from lateral flow between the tunnel inflow points and the valley floor. Nonetheless, the actual fluid pathways and the processes driving infiltration against regional hydraulic gradients were unconsidered prior to this study.

3 Methods

We mapped the brittle deformation features associated with hydrothermal activity at Grimsel Pass in detail during the 2014 field season. In addition to major Alpine mylonitic SZs previously mapped and modelled in 3D by Baumberger (2015) and Wehrens (2015), we traced further, subordinate lineaments potentially pertinent to this study (Fig. 3). Lineament tracing was implemented by fusing orthophotos and 2 m resolution digital elevation models with multiple hillshade illumination angles. These lineaments are inferred to trace ductile SZs or brittle faults that are preferentially susceptible to erosion and morphological incision. The remotely traced structures are mostly not field-validated, so their exact nature and paragenesis is mostly unclear. However, Baumberger (2015) and Wehrens (2015) demonstrated that the vast majority of the lineaments in the Grimsel Pass area correlate with fault zones. Subsurface projection of the GBF was implemented in Midland Valley's Move™ software and integrated into projections of the regional SZ network by Baumberger (2015). Projection relied on the intersection of the fault surface trace with the steep topography (Woodcock 1977; Fernández 2005; Baumberger 2015), the logged breccia

intersection in the Transitgas tunnel (Schneider 1974), and surface dip measurements. The resulting 3D model is not the focus of this study, but a first approximation to facilitate discussion.

Stereoplots (Fig. 4) were generated in “Stereonet9” (Allmendinger 2014). Mean principal orientations of the master fault were calculated in Midland Valleys Move™ software. All master fault orientations are taken from discrete, late fault planes cutting or bounding the fault-core breccias.

Mineralisation associated with the GBF (Hofmann et al. 2004) was mapped from the onset of distinctive secondary silica void coatings or fillings (Fig. 5d, e), whereas stained fracture surfaces (from sub-recent oxidation of iron sulphides) lacking secondary silica were ignored. Where repeatedly present at the outcrop scale, mineralisation is mapped as ‘mineralised outcrop’. These zones, as well as isolated traces of mineralisation too small to show on Fig. 3 are linked and encompassed by the ‘mineralisation extent’, outside of which no mineralisation was observed.

In order to quantify macroscopic fracture network properties, line-intercept-discontinuity analyses were performed approximately normal to the fault in areas with the best outcrop availability. Intersections and the apertures of joints and faults as well as ‘no-outcrop’ lengths were recorded. Apertures were recorded from wall rock to wall rock, ignoring mineralisation or infill, and thus represent the maximum possible aperture if no mineralisation or tectonic closing had occurred. No correction was made for orientation biases (e.g., Terzaghi 1965; Mauldon et al. 2001). Incomplete outcrop (summarised for the entire line in Table 1) obscures measurement of some recessive SZs, and aperture measurements at the surface are probably somewhat higher than at formation depth due to exhumation and pressure reduction (Morrow and Lockner 1994). The data were grouped into 5 m bins centred every 2.5 m away from the fault core. A 5 m bin size was chosen to reflect fault-zone scale progressions while maintaining representative mean values. To account for intervals with no outcrop, the discontinuity count was scaled according to the outcrop proportion within the individual bins, and converted to counts per meter for the entire bin.

4 Results

4.1 Structural geology of the Grimsel Breccia Fault

The GBF was mapped along a total strike length of 4.6 km between Gletsch and the Trübtensee (Fig. 3), though may continue under Quaternary cover at either end. The fault cuts the SWAGr and crosses into the Grimsel Zone at the north ridge of the Sidelhorn. The GBF core varies from

0.2–2 m thick discrete fault breccias to zones up to 5 m thick with multiple anastomosing strands of fault breccia and fractured rock. For at least 3 km through the central and eastern sections (Fig. 3: from positions B–F), the GBF closely overprints a major mylonitic Alpine SZ (Fig. 3: GSZ 1). 500 m east of the Sidelhorn north ridge (Fig. 3: position B) the master fault links to the WNW. This linkage laterally steps the fault 300 m over approximately 1000 m strike length in what we term the Sidelhorn linkage zone (Fig. 3: position A). The presence of a secondary fault is inferred to continue under Quaternary cover WSW along GSZ 1 for at least 600 m to outcrop at the ridge, marking the southern margin of the linkage zone. Fault surface striae and tectonic brecciation in the linkages, as well as a 10°–15° juxtaposition of foliation orientations either side of the fault core indicate that the linkages are brittle shear structures that bend the master fault, not purely extensional jogs and dilational breccias.

The GBF orientations are split into two sets according to their position on different fault segments (Fig. 4a). The ‘Main orientations’ plotted in Fig. 4 are modal, and strike approximately WSW-ENE, sub-parallel to Alpine ductile SZs, whereas linking orientations strike approximately E-W to WNW-ESE. The mean principal orientations of these two sets make a 25° angle with each other, though a range of intermediate values exists. Surface measurements and 3D modelling (Figs. 3, 4a) indicate that the GBF plane dips steeply throughout (80°–90°). However, the master fault plane, as well as GSZ 1, gently twists from a slight south dip (85° S-SSE) along the western section, to a sub-vertical central section (88° SSE), to a slight north dip along the eastern section (85° NNW). These orientations are, within error, in agreement with 3D models of GSZ 1 by Baumberger (2015). Notable dip deviations as shallow as 73° SSW occur along select fault linkage outcrops between positions A and B (Fig. 3).

Shear zones with similar orientations to the fault linkages exist elsewhere in the field area, as part of the regional SZ network (Wehrens 2015). However, the largest linking segment (between positions A and B in Fig. 3) cuts through weakly schistose granite separating high strain GSZs 1 and 2. Ductile deformation is expressed relatively weakly and homogeneously directly either side of this linkage structure. Any potential ductile precursor linkage, if at all present, must therefore have had a total width less than the 1.5 m wide morphological incision obscured by quaternary sediments, therefore being significantly subordinate to the >10 m wide strained zones surrounding GSZs 1–4.

Quaternary cover obscures a continuous GBF trace between Grimsel Pass and Gletsch as it approaches the SZ4 separating the SWAGr and the Ausserberg-Avat Zone (between positions E and F in Fig. 3). However, isolated mineralised faults (also mapped by Hofmann et al. 2004)

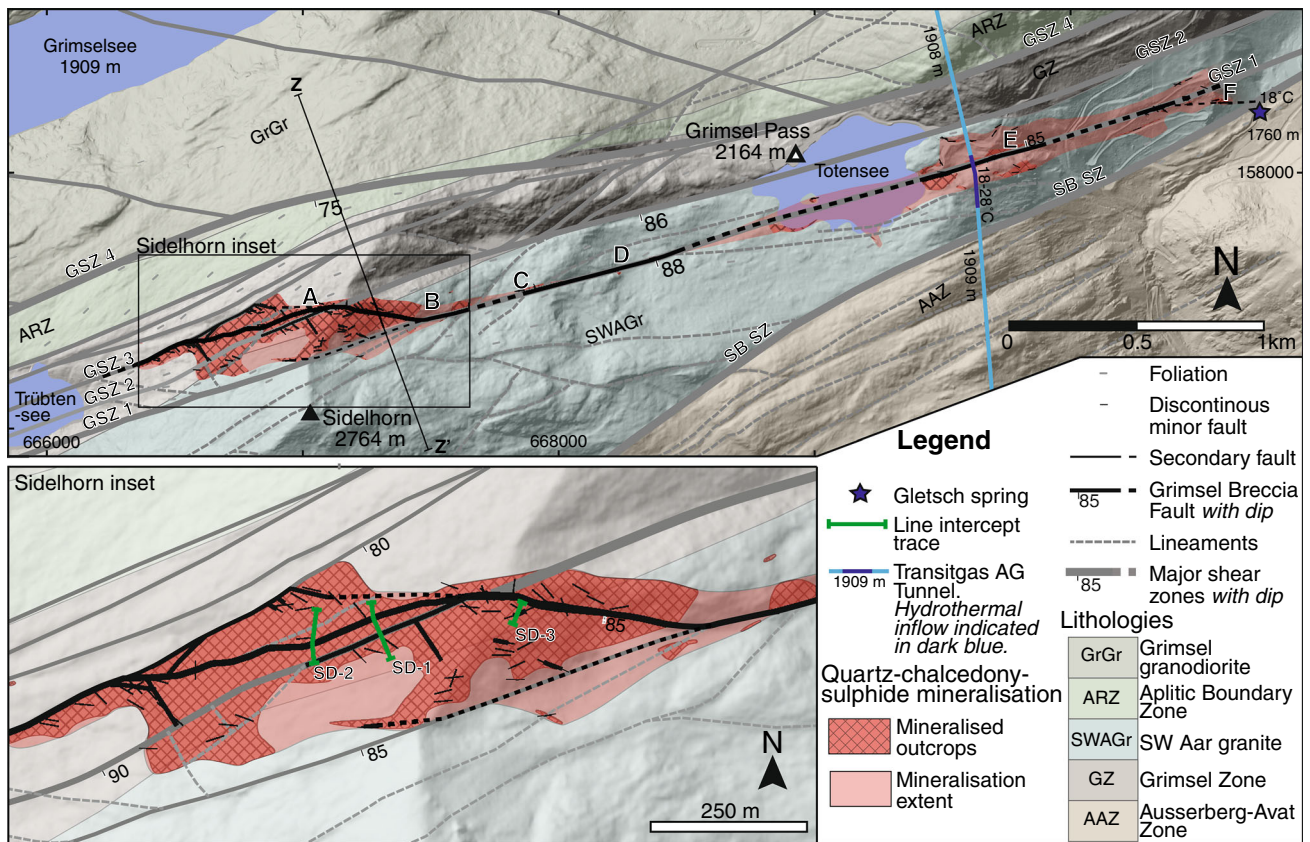


Fig. 3 Map of the Grimsel Breccia Fault zone, its mineralisation and geological environment. Positions A–F, Grimsel Shear Zones (GSZ) 1–3, the Southern Boundary Shear Zone (SB SZ) and line intercept traces SD 1–3 are referred to in the text. The tectonic foliation is steeply dipping ($>70^\circ$) throughout the study area. Shear zone/fault plane dips are indicated along traces. Mineralised outcrops are defined by ubiquitous mineralised fractures and void space. Mineralisation

extent traces the outline of the mineralised outcrops as well as discreet traces of mineralisation too small to represent here. Lines are dashed where inferred. See text for further methodology. All altitudes in metres above sea level. Lithologies are modified after Stalder (1964), Abrecht (1994), and Wehrens (2015) and major SZs are drawn after Baumberger (2015) and Wehrens (2015)

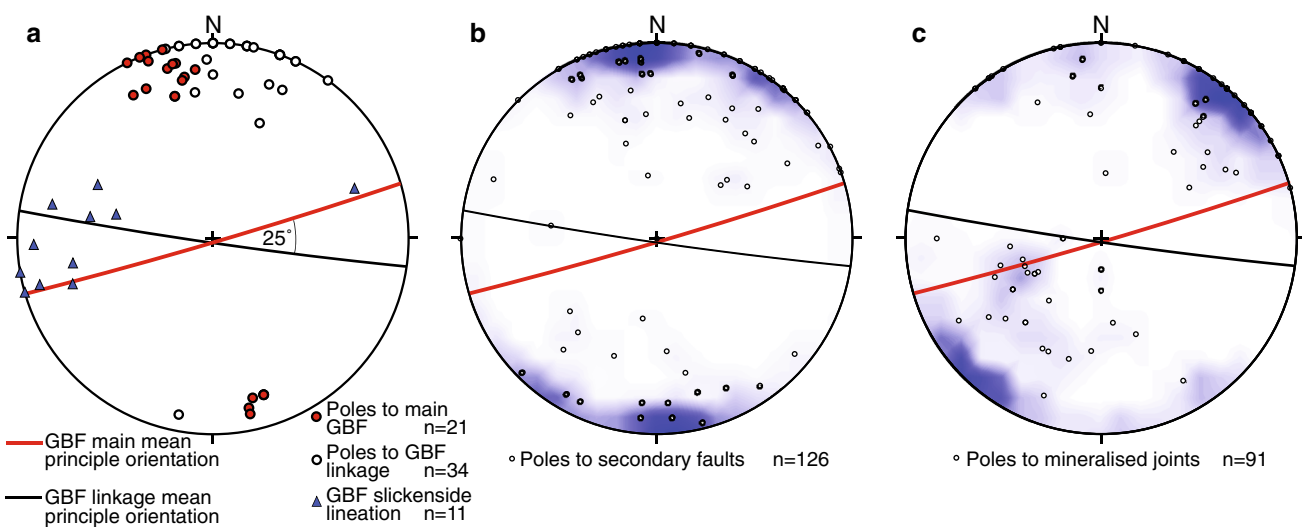


Fig. 4 Stereoplots (Schmidt, lower hemisphere). **a** Poles to GBF master fault orientations and slickenside lineations. **b** Poles to secondary faults of the GBF system. **c** Poles to mineralised joints.

Contouring by the Kamb (1959) method in Stereonet9 software (contour interval of 0.5, significance of 1.25 sigma, grid spacing of 20; Allmendinger 2014)

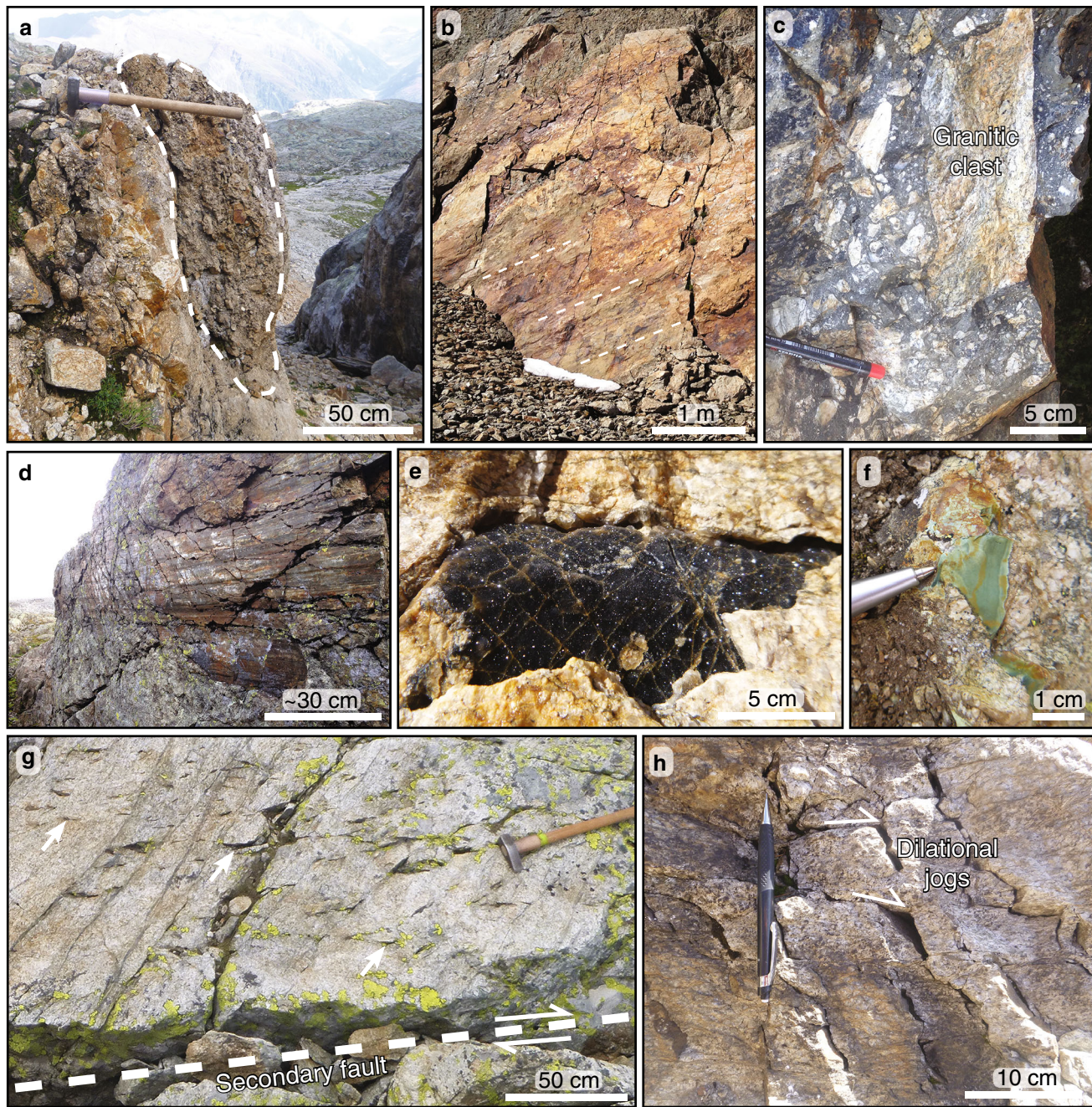


Fig. 5 Field photographs of the GBF zone. (Locations given in Swiss national grid format). **a** 50 cm thick core breccia lining recessive lineament on major Sidelhorn fault linkage (2667245, 1156454). **b** Looking north at a late fault plane (dip direction 190°, dip of 80°) in the GBF core with slickensides dipping ca. 30° W (2667429, 1156426). **c** Microcrystalline quartz-cemented breccia with granitic clasts lining a recessive lineament (ca. 2666670, 1156400). **d** Fault surface (dip direction 190°, dip of 70°) in secondary breccia with 17°

W dipping slickensides (2666422, 1156263). **e** Typical coarse quartz-sulphide mineralisation at the north ridge of Sidelhorn (2667170, 1156470). **f** Irregularly shaped celadonitic chert infill between Totensee and Gletsch (2670294, 1157235). **g** 3 m wide mineralised damage zone around 10 cm thick secondary fault, ca. 10 m from the GBF core at the north ridge of Sidelhorn (2667155, 1156464). **h** Dilatational jogs/fractures with quartz-sulphide coatings, 5 m from the GBF core on the NW slopes of the Sidelhorn (2667121, 1156479)

crop out 200 m WNW of Gletsch with a strike of ca. 100° (Fig. 3: position F), suggesting that a strand of the GBF may link south to the major SZ4, in a similar orientation to other linkage structures described above.

Secondary brittle faults are subordinate in thickness and length to the master fault. The secondary fault orientations cluster similarly to the GBF main and linking orientations, with similar dip ranges (Fig. 4b). However, the overall

spread of strikes is greater, with orientations varying from NW–SE to NE–SW. Mineralised joints lacking evidence for shear displacement (e.g., striae) are presented in Fig. 4c and show a similar, though slightly wider range of orientations to the secondary faults. Compared to the secondary faults, the joints strikes show a similar spread from NW–SE to NE–SW, between 10–60° to the master fault orientations; however, the majority of joints make a steeper angle (50–80° clockwise) to the main GBF orientation. Additionally, lower angle joints exist, dipping towards the NE quadrant at between 10–70°.

Occasionally, late, striated faults with microcrystalline quartz slickenfibres and mechanical striae cut through the master fault breccias (Fig. 5b, d). These lineations cluster between 35° W and horizontal, with a mean of 268°/15°. Fault surface accretion steps and mineral fibres, R-orientation secondary structures (Fig. 4b), and preferential striation of fault surfaces facing the direction of movement (PO-type striation; Petit 1987) observed during this study all agree with the dextral shear sense for the GBF reported by Hofmann et al. (2004).

Useful passive markers for estimating displacement are scarce along the GBF due to generally low intersection-angles and uncertain paragenesis of most potential markers. However, rare passive marker offsets indicate a dextral slip sense for the GBF. In the central section of the GBF, two lineaments are cut by the GBF at ca. 30°, recording a dextral, strike-slip offset of 25–45 m (Fig. 3: position C). The significant uncertainty in this value results from 5–10 m of Quaternary cover either side of the inferred GBF trace, and the possibility of curvature into the ductile SZ. The easternmost offset structure exhibits horizontal striae in a biotite-coated fault surface. This characterises the marker as an Oberaar phase structure, recording strike-slip deformation at biotite-stable temperatures (Wehrens 2015). Therefore, this feature certainly pre-dates the cooler brecciation along the GBF (Hofmann et al. 2004). However, this offset integrates the total strike-slip movement along the SZ since the marker formed, not the offset specifically associated with the hydrothermally influenced breccias. Accordingly, it does not constrain a reliable minimum displacement for deformation associated with the GBF. However, this offset does point towards a maximum strike-slip displacement of ca. 45 m along the central GBF. At the Sidelhorn north ridge (Fig. 3: position A) the GBF obliquely cuts the highly sheared intrusive contact between the Grimsel Zone and SWAGr. Here, both units consist of pervasively sheared orthogneisses that are difficult to distinguish and use as markers in the field. Within the Grimsel Zone, internal structures (SZs, dykes, intrusive contacts) cannot be readily traced on both sides of the main GBF trace.

4.2 Field relationships to alpine mylonitic shear zones

For 3.4 km out of the 4.6 km mapped strike-length, the GBF trace clearly coincides with major WSW-ENE striking GSZs 1 and 3 (Fig. 3). Where SZ cores are brittlely overprinted they are usually morphologically incised and often covered by quaternary sediments. From the limited complete exposures available, the breccia's actual position within the SZ architecture appears to be variable, moving from the centre to both the northern and southern protomylonitic margins of the SZs. In the steep gully east of the Totensee (Fig. 3: position E), core breccias overprint the mylonitised southern SZ margin as a 0.5–1 m thick, cemented coating on the wall. Farther down the gully, 50 m to the ENE (grid reference 2669835, 1157090), the breccia overprints a rare complete outcrop of the 1.5 m wide SZ core, with cemented breccias either side of a ca. 0.3 m thick, weakly cohesive fault gouge. Contrastingly, 160 m below and 200 m to the west at the tunnel intersection, logs indicate the breccia overprints the northern margin of the SZ (Schneider 1974).

4.3 Extent of mineralisation

Mapping of epithermal mineralisation associated with the GBF reveals order-of-magnitude along-strike variability in the extent of mineralisation around the fault (Fig. 3). Two major mineralised fault segments are identified: the Sidelhorn Linkage Zone, 200–300 m wide and extending over 1000 m; and the Grimsel Pass-Gletsch Zone, ca. 200 m wide and extending at least 2000 m from the Totensee to position F on Fig. 3 (where quaternary cover obscures further tracing). These zones are separated by a ca. 1.5 km along-strike stretch of limited mineralisation from position B (Fig. 3) to the western shores of the Totensee. In this limited zone, mineralisation is restricted to a few metres either side of- or exclusively to the master fault core.

Mineralisation is associated with a higher density of damage zone secondary breccias and faults. At the north-western margin of the Sidelhorn linkage zone, mineralisation is delimited by a 5–10 m wide mylonitic SZ (Fig. 3: Sidelhorn Inset). Fracture networks exist in the host rocks either side of this SZ, however along this section, on the NNW side, they are either unmineralised or biotite-coated. Similar SZs of varying widths exist sub-parallel to the GBF throughout the field area. A second order of mineralisation heterogeneity is observed at the decametre scale, as shown by 'Mineralised outcrop' zones in well exposed areas on the Sidelhorn's slopes (Fig. 3): with an abundance of mineralised fractures relative to adjacent outcrop.

4.4 Sub-thermal discharge

Sub-thermal fluid discharge was measured in July 2014 over an interval of 50 m in the Transitgas AG Tunnel, centred on the highest temperature 28.2 °C inflow. This inflow coincides with the logged tunnel-GBF intersection within the projection error (Schneider 1974). Within this broad zone, discharge is discontinuous, with multiple distinct inflow points. However, measurements from 1974 (Schneider 1974), and 1992 (Pfeifer et al. 1992) document discharge with elevated Na, SiO₂, Cl, SO₄ contents and temperatures between 18 and 28 °C over a much wider interval of ca. 300 m, including up to 170 m south of the GBF intersection (Fig. 3). Interestingly, the spring at Gletsch, though not necessarily at the exact bedrock discharge point, roughly correlates with the potential GBF linkage to SB SZ.

4.5 Line-intercept fracture analyses

Fracture locations and aperture were recorded along three profiles approximately normal to the master fault trace at three different points in the Sidelhorn linkage zone (Fig. 3: Sidelhorn inset). Because of their position within the linkage zone, and ubiquitous brittle deformation around Grimsel Pass (hydrothermally overprinted or otherwise), it is important to note that the examined lines do not extend into true ‘background’ fracture networks. However, fracture density minima consistently fall around 1–2 fractures per m: an effective background value for the Grimsel Zone in the area. Each line has slightly different immediate lithological and structural surroundings (Table 1) and a complex fault architecture. Due to these particularities, the data do not allow detailed comparison with other similar faults. Measured fracture density values vary from 1 to 11 fractures per metre and mean apertures vary from 0 (a closed seam) to 2.9 mm (Fig. 6). In all three lines, we see the highest fracture densities from 0–15 m either side of the fault core. Asymmetry in fracture density around the fault core is most pronounced over line SD-1, with higher fracture densities in the less foliated block to the south. Elevated mean apertures also spatially correlate with the fault core. However, these elevated apertures peak 10–15 m from the fault core, with stronger asymmetry than the fracture density distribution (Fig. 6).

The cores of major SZs intersected by the lines generally form recessive lineaments, filled with Quaternary

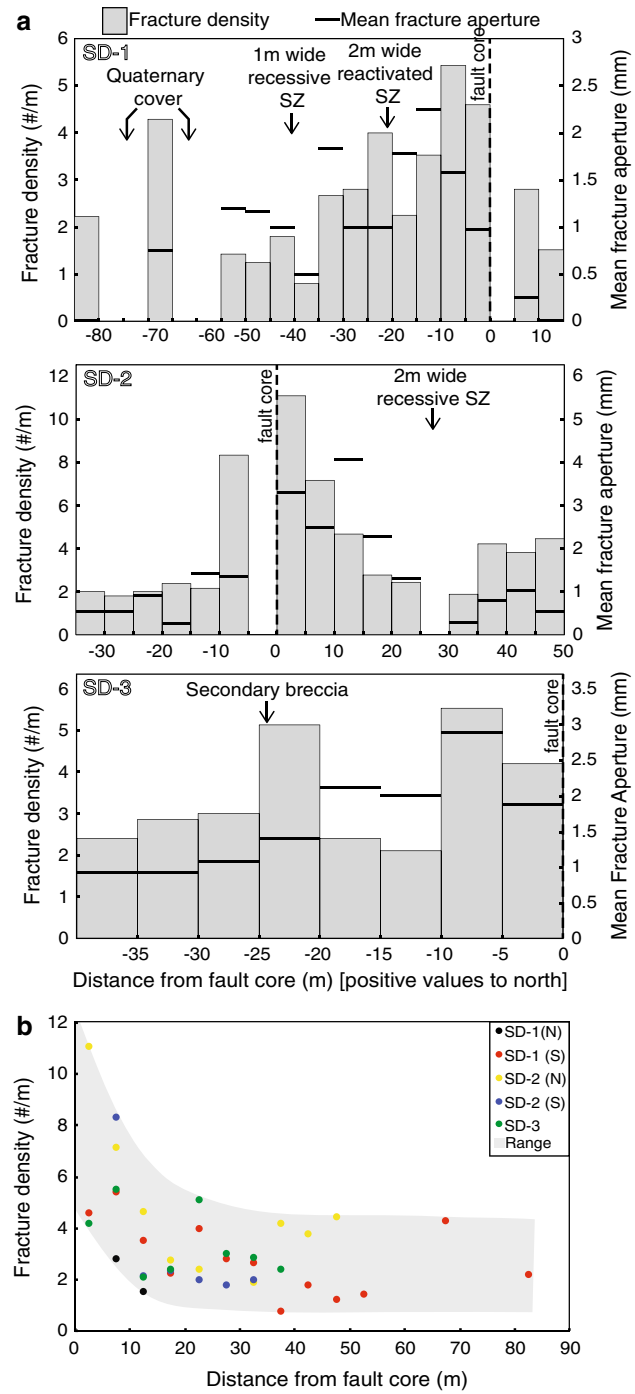


Fig. 6 Line-intercept discontinuity analyses. **a** Individual lines. **b** Summary plot. *Line traces* are marked on Fig. 3. Positive values of distance from the fault core are to the N side. Empty columns correspond to no outcrop over that interval

Table 1 Outcrop availability and lithological summary for line intercept analyses SD-1–3 (Fig. 6)

Line	Outcrop %	General lithology
SD-1	62 %	Moderately foliated orthogneiss, stronger to north
SD-2	57 %	Moderately to strongly foliated orthogneiss
SD-3	84 %	Weakly but pervasively foliated granitic orthogneiss

sediments, preventing access. Despite the lack of direct data on many of these SZs, fracture density is seen to both decrease (SD-2) and increase (SD-1) to either side. By tracing the SZs along strike to better outcrop, it appears that increases in fracture density occur where the SZs are overprinted by the GBF system, and decreases where no obvious overprinting has occurred.

4.6 Microstructures

The petrographic characteristics of the breccias have previously been described in detail (Hofmann et al. 2004). We present selected features relevant to the structural characterisation of the GBF system (Fig. 7). Distal to the fault core (Fig. 7d: 34 m from fault core) a strong foliation in gneiss is defined by recrystallised quartz and aligned micas, banded in varying thicknesses. Similar banding occurs in outcrop at the decimetre-scale, defined by multiple strands of mylonite separating lower strain orthogneiss. At both scales, the felsic bands are preferentially jointed, with

joints often delimited by the micaceous bands. Despite being within the mineralised zone of the GBF, some open fractures within the strongly foliated rock are free of mineralisation (Fig. 7d). The across-foliation joint orientation in Fig. 7d corresponds with the dominant orientation of mineralised joints shown in Fig. 4c.

Rebrecciated textures are ubiquitous in the GBF core breccias. Samples of the fault-core breccias usually record at least three widely distinguishable generations of deformation, porosity creation and subsequent mineralisation. First generation breccias consist of host rock components in various stages of mechanical decomposition. These form two end-member breccia types: one clast-supported in a matrix of milled rock (Fig. 7a), and one supported by microcrystalline quartz cement, stained dark grey by finely milled rock, sulphides and minor hydrothermal clays (Hofmann et al. 2004). This first-generation cemented breccia is a common clast component in second-generation breccias (Fig. 7b, c). Typical third generation deformation fractures these clasts discretely without significant rotation

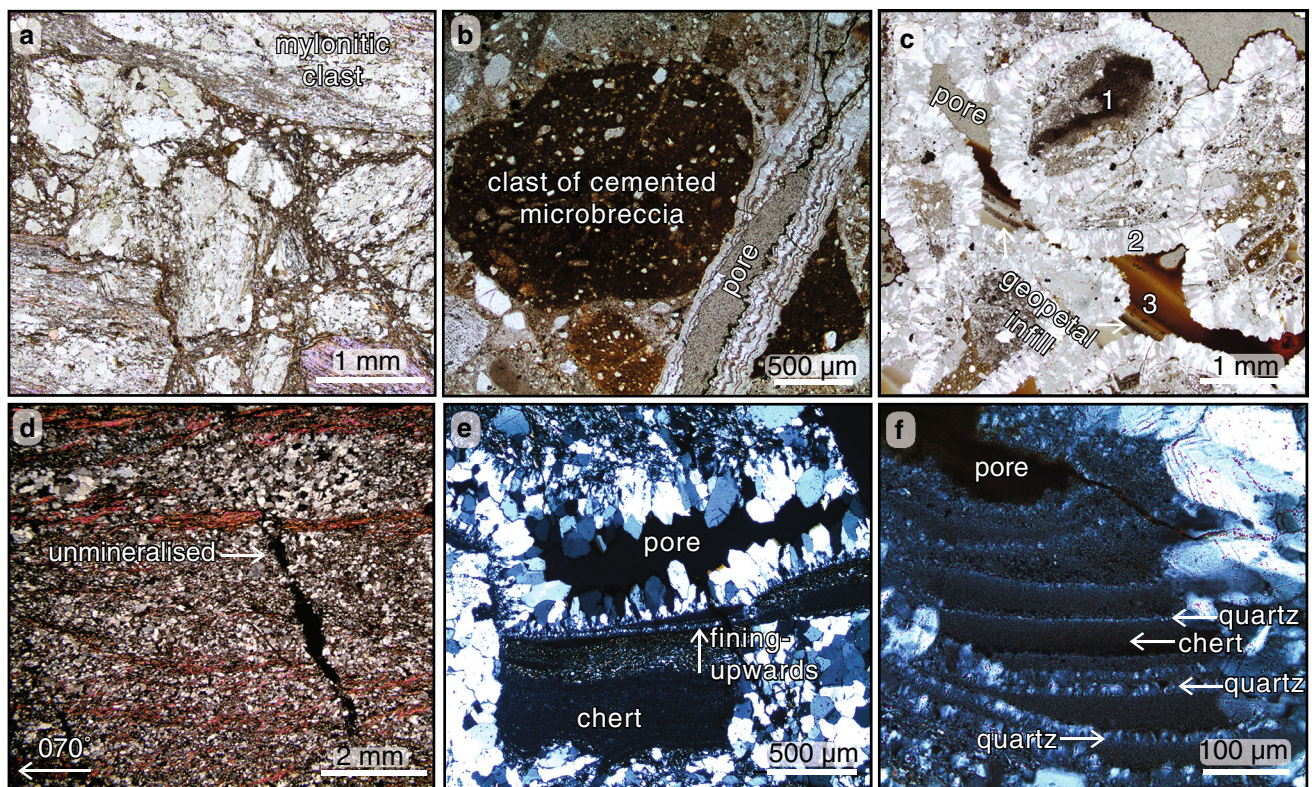


Fig. 7 Microstructures of the GBF. **a** Unmineralised, clast-supported breccia with angular clasts of mylonite in a matrix of finely milled rock (GR17). **b** Prominent dark clast of sulphide-stained microcrystalline-quartz-cemented microbreccia (first generation) rebrecciated in light grey matrix (second generation) and subsequently discretely fractured (third generation) and incompletely mineralised with zoned quartz (GR22). **c** Breccia supported by clasts of grey-black, microcrystalline-quartz-cemented cataclasite (1), with comb quartz (2)

partially occluding interclast porosity and late, brownish geopetal cherty infills (3), (GR22). **d** Small, unmineralised fracture within the mineralised zone, 34 m from the master fault, in strongly foliated gneiss of the Grimsel Zone (SD-14-11) **e** Fine grained chert infill with upwards-fining geopetal cap (see arrow), overgrown by comb quartz, evenly around the pore (GR35). **f** Geopetal banding of quartz and chert in a pore with at least eight discernible quartz bands (GR35)

(Fig. 7b), allowing zoned comb quartz and occasional adularia growth on the fracture surfaces. Within breccias that overprint SZs, clasts of proto-mylonitic host rock are common (Fig. 7a).

The latest phase of mineralisation along the western and central sections of the GBF consists of brownish, cherty geopetal infills (Fig. 7c; see also Hofmann et al. 2004). These stratification orientations are consistent throughout individual samples and often compatible with present-day outcrop orientations. Along the eastern section of the fault, very fine-grained celadonitic chert mineralisation (Fig. 5f) appears to be the latest phase of quartz mineralisation. This texturally distinct mineralisation grows directly on wall rock, apparently into newly created space.

5 Discussion

5.1 Interpretation of quartz varieties

Solubility is prograde within the amorphous silica-chalcedony-quartz system, but decreases with increasing degree of crystallinity (Rimstidt 1997). It follows that macrocrystalline quartz growth is favoured at higher temperatures than micro- or cryptocrystalline varieties. Brecciation along the fault occurred in a steadily exhuming (cooling) environment (Glotzbach et al. 2010). However, in the GBF core breccias, coarse-grained comb quartz commonly overgrows: (1) microcrystalline quartz cemented breccias (Fig. 7b, c), and (2) geopetal chert infills and bands (Fig. 7e, f). This timing sequence (microcrystalline quartz first, then macrocrystalline) can be explained by changes in fluid properties over time, and we suggest different mechanisms for each respective circumstance.

1. Breccias with angular clasts supported by very fine grained cement (Fig. 5c; Fig. 7c, dark clast) are often attributed to sudden co-seismic pressure drops, saturating the fluid with respect to silica and quickly precipitating the supporting cement (Sibson 1986). In this case, coarse-crystalline quartz growth was inhibited by its sluggish precipitation (Morey et al. 1962; Rimstidt 1997), but resumed when pore fluid pressure returned to background levels, coating the remaining pore space. Reworking of the cement-supported breccias (Fig. 7c) as second-generation clasts indicates that these processes were active early in the GBF's development. Apart from this suggestion, no substantial evidence (Rowe and Griffith 2015) was found for seismic slip along the GBF.
2. Macrocrystalline comb quartz both overgrows (Fig. 7e), and is sequentially banded with (Fig. 7f) geopetal chert infills. The pore infill on Fig. 7f records

at least eight such alternating bands, indicating episodic fluctuation of the fluid between macro- and microcrystalline quartz favoured conditions. Pulses of fluid with different temperature, composition or both can explain this sequencing. The presence of macrocrystalline quartz shows that, under quiescent conditions, the wall rock temperature was high enough to stabilise quartz. In light of this, the fluctuations in silica crystallinity can be explained by intermittent pulses of fluid oversaturated with respect to amorphous silica and microcrystalline quartz. These pulses precipitated the fine geopetal chert layers until the fluid reached saturation of the lower-crystallinity phases and their precipitation halted. Macrocrystalline quartz however, remained supersaturated in the ascending fluid and continued to precipitate evenly around the pores. This interpretation is supported by the ubiquity of macrocrystalline quartz as a late pore coating throughout the GBF mineralised zone (Fig. 5e).

5.2 Structures of the Grimsel Breccia Fault

5.2.1 Inherited geometries

Reactivation and brittle overprinting of Alpine mylonitic GSZs 1, 2 and 3 by the GBF is clearly shown by map-scale spatial relationships (Fig. 3) and microstructural observations (Fig. 7a). GSZ 1 was reactivated by the GBF over at least 3 km strike length. Ductile shearing occurred along GSZ 1 until ca. 13 Ma (Rolland et al. 2009), and along regional SZs until ca. 7 Ma (Fourcade et al. 1989; Chalandes et al. 2008; Rolland et al. 2009; Bergemann et al. 2014). The purely brittle deformation accompanying Pliocene hydrothermal activity in the GBF clearly post-dates the dominantly ductile processes that formed the SZs at greenschist facies conditions. This timing is corroborated by overprinting relationships from mapping and microscopy (Figs. 3, 7a), and is logical in a steadily cooling environment (Glotzbach et al. 2010).

The mineralisation age of 3.30 ± 0.06 Ma calculated by Hofmann et al. (2004) derives from a late adularia overgrowing a breccia clast in the Sidelhorn linkage zone, and may post-date brecciation entirely. Given this single age constraint, it is permissible that deformation occurred much earlier than 3.3 Ma: perhaps continuously since the next youngest regional deformation dated at ca. 7 Ma (Bergemann et al. 2014). Moreover, continued deformation post-dating the main phase of mineralisation is suggested by weakly cohesive fault gouges cutting microcrystalline quartz-cemented breccias east of the Totensee. Further strongly localised, late deformation along GSZ 1 cannot be ruled out, as the SZ is invariably recessive, with its core

and any potential gouges generally obscured by quaternary cover.

Neogene embrittlement of ductile SZs during exhumation has been described throughout the Aar and Gotthard massifs (Zangerl et al. 2006; Rolland et al. 2009; Campani et al. 2010; Baumberger 2015; Wehrens 2015). The mechanical and geometrical SZ properties that promote this reactivation are a direct result of the Alpine evolution at Grimsel Pass, as summarised below after Wehrens (2015).

Alpine SZs in the Aar massif preferentially initiated on pre-existing mechanical anisotropies such as lithological contacts, sheet-silicate rich zones, meta-basic or aplitic dykes or high-temperature fractures in relatively isotropic rocks (e.g., post-Variscan plutons). During strain accommodation at greenschist facies conditions, grain size reduced from 1–2 mm in granitic protoliths to as small as a few μm in the ultramylonitic SZ cores (Wehrens 2015). Accompanying this grain size reduction, Wehrens (2015) interprets that dynamic recrystallisation, alignment of sheet-silicates, and the precipitation of new phases progressively isolated porosity in the SZs and consequently decreased permeability. Nevertheless, fluid access was maintained by brittle fracturing, facilitating alteration of feldspars to sheet-silicates (Wehrens 2015). Relative to their lesser-deformed host plutons, this alteration locally increased the proportion of sheet silicates within the SZs, while concurrent deformation forced their alignment. Combined, these processes resulted in structural and reaction weakening of the SZ cores, forcing both ductile and ensuing brittle deformation to localise into discrete planes (Wehrens 2015).

Despite major kinematic progressions during the Cenozoic, these SZs have been repeatedly exploited by the Handegg phase, the Oberaar phase and exhumation-related, late stages of Alpine tectonics (Rolland et al. 2009; Wehrens 2015), with each deformation phase exploiting and subsequently reinforcing the mechanical discontinuities. Our investigation shows that the GBF largely adheres to this trend of reactivation, though localised departures exist in the form of fault linkages between segments of reactivated SZ.

5.2.2 Kinematics

The apparent dextral strike-slip offset of 25–45 m (Fig. 3: position C) and a mean 15° lineation plunge corresponds to a heave of 7–12 m and a maximum displacement of 26–47 m along the central section of GBF.

Late Alpine, dextral strike-slip faulting along and north of the Rhone Valley is kinematically similar to the GBF (e.g., Hubbard and Mancktelow 1992; Campani et al. 2010). Stress estimates indicate this ongoing faulting is driven by NW–SE

oriented maximum horizontal stress ($S_{H\max}$), resulting from continued continental convergence and anti-clockwise rotation of the Adriatic plate (Hubbard and Mancktelow 1992; Maurer et al. 1997; Pleuger et al. 2012). Although no fault-plane paleostress analysis was made during this study, tensile joints should preferentially form perpendicular to the minimum stress orientation, and strike parallel to the maximum horizontal stress (Kranz 1983 and references therein). The strikes of mineralised joints surrounding the GBF (Fig. 4c) group between 120° and 145° . This orientation is remarkably consistent with a NW–SE oriented $S_{H\max}$ derived from fault-plane analysis of active faults 50 km to the west (Maurer et al. 1997). Due to the close inheritance of pre-existing SZs, the GBF's orientation is strongly preconditioned, and therefore cannot be an ideal kinematic representation of regional stresses (Bistacchi et al. 2012).

Slickenside measurements indicate a slightly up-thrown northern block, which is in agreement with Hofmann et al. (2004), but contrasts with the prevailing south-block-up kinematics of earlier deformation phases at Grimsel Pass (Rolland et al. 2009, Wehrens 2015). However, striated fault surfaces clearly post-date initial brecciation and cementation (Fig. 5d). The lack of macrocrystalline quartz on these surfaces, where otherwise abundant in the adjacent damage zone, suggests the kinematic record is only well preserved for relatively late slip. Assuming no significant tilting has occurred since the Pliocene (Glotzbach et al. 2010), this slight up-throw of the northern block can be interpreted as both a slight normal component along the south-dipping western half of the GBF, and a slight reverse component along the north-dipping Grimsel Pass-Gletsch Zone. The (late?) north-block-up component may express an exhumation gradient at the southern boundary of the Aar massif or be related to variations in exhumation rates contemporaneous with the hydrothermal brecciation (Vernon et al. 2009).

5.2.3 Fault linkages

Over the Sidelhorn linkage zone, three fault segments (reactivations of GSZ 1–3) are arranged sub-parallel to each other, connected by fault linkages (Figs. 1, 8). Surrounding the linkages is a mesh of secondary faults and dilatational breccias (the Sidelhorn linkage zone). The fault

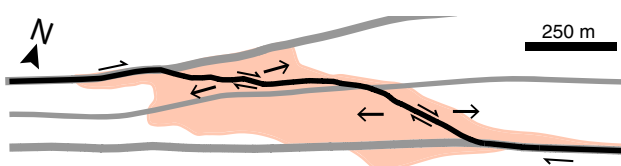


Fig. 8 Sidelhorn linkage zone sketch. Localised dilatancy and therefore increased porosity and fluid access occur on the fault linkage

linkages pose two interrelated questions: (1) what forced the linking faults to depart from the reactivated SZs, and (2) what controlled the resultant linkage geometry?

Where the orientation of pre-existing mechanical anisotropies was compatible with the stress field during formation, reactivation should occur, as is seen in the central and eastern GBF. Conversely, as the orientations of pre-existing anisotropies diverges from the compatible failure plane, or vice versa by stress re-orientation, reactivation will eventually switch to more compatible sets of anisotropies, or cease in favour of novel fault propagation. However, GSZ 1 and GSZ 2 do not markedly change orientation at their respective linkage points. This suggests another initiation-trigger, which is not clear from our data. Possible candidates are internal structures within the Grimsel Zone, or along-strike variations in SZ strength. The resultant geometry of the fault linkages provides insight into the tectonic context requiring their formation. We suggest two possible mechanisms:

1. With the onset of dominantly brittle deformation, Riedel-orientation secondary faults formed around the formerly ductile SZs. Eventually, these Riedel shears connected and linked between SZs, with the unconnected shears preserved as discontinuous faults in the linkage zone.
2. ‘Weak’ faults are known to slip under high angles ($>60^\circ$) to maximum principle stress (Byerlee 1978; Hardebeck and Hauksson 1999). However, segments of the GBF propagated into relatively undeformed crystalline rocks are more likely to adhere to ideal geometries. A NW–SE oriented $S_{H\max}$, as supported by mineralised joint cluster orientations (Fig. 4c), makes a reasonable angle with ‘weak’ reactivated segments (ca. 62°) and also ‘strong’ inter-SZ linkages (ca. 35° ; Byerlee 1978). In this case, displacement along the unfavourably oriented SZs would have been possible due to their marked mechanical weakness relative to the host rocks (Bistacchi et al. 2012). Contrastingly, the largest fault linkage propagated across foliation into relatively isotropic inter-SZ SWAGr host rock, with close to ideal orientations relative to the regional stresses.

If a NW–SE $S_{H\max}$ interpretation is correct, fault-normal stress would be much higher along the reactivated SZ segments than the fault linkages, with possible implications for fault surface sealing and the restricted fluid access observed along the central section of the GBF.

5.2.4 Fault architecture

Fault architectural models of fluid flow can be simplified into three components: undeformed protolith, damage zone

and fault core; with the relative properties and extent of each exerting first order control on the resultant hydraulic architecture (Chester and Logan 1986; Caine et al. 1996). The decimetre to metre-scale brecciated core of the GBF, apparently uncommon in the Aar massif, requires specific tectonic and hydrologic formation conditions. Sibson (1986) describes three modes of brecciation and indicates that all three may operate in long-lived systems. We find evidence for all three in the GBF: (1) Attrition brecciation by fault slip in the absence of a mineralising fluid (Fig. 7a). (2) Distributed crush-brecciation in lesser-deformed lenses between anastomosing fault core strands. (3) Implosion brecciation, forming clearly hydrothermal breccias in dilatational space, supported in cementing mineralisation (Fig. 5c).

Damage zone width varies by an order of magnitude along-strike, from the 100 to 300 m wide Sidelhorn linkage zone and Grimsel Pass-Gletsch Zone, to the 5–30 m wide central section (Fig. 3: note variable secondary and discontinuous fault distributions). In low-porosity crystalline rocks, fracture density, aperture, and shape, are the most important controls on permeability (Stober and Bucher 2007). Consequently, the fracture distributions we measure are a first order control on naturally enhanced permeability distribution around the GBF.

Damage and associated permeability surrounding faults is understood to decay with distance from the fault core, dependant on lithology, fault architecture and the tectonic environment (Vermilye and Scholz 1998; Janssen et al. 2001; Rawling et al. 2001; Mitchell and Faulkner 2009; Savage and Brodsky 2011). Line-intercept analyses of the damage-zone macrofracture network (Fig. 6) show that this relationship generally holds for the GBF. Both fracture density and mean aperture decrease with distance from the GBF core. Consistent minima of 1–2 fractures per metre mark the effective background fracture density within the Sidelhorn Linkage zone. Around the proto-mylonitic margins of select SZs, fracture density appears to drop. Conversely, where reactivated as a brittle fault, fracture density increases around the SZs. The different lines expose along-strike differences in the GBF damage-zone fracture network, both in terms of properties and their relative distributions. Contrasting lithologies and foliation intensities (Table 1) hint at the lithological controls on the fracture network. On line SD-1 (Fig. 6a), fracture density is strongly asymmetric and drops sharply to background levels over 10–15 m in the strongly foliated northern block, in comparison to over at least 35 m in the southern, less foliated block.

Fault architecture is strongly influenced by local geometric variations along faults (Shipton and Cowie 2001; Shipton et al. 2005), and our mapping demonstrates that this relationship applies to the GBF. The most extensive

damage around the master fault coincides with the Sidelhorn linkage zone, which is the most significant geometric complexity mapped along the GBF. Another possible influence on the distinct fault architecture at the Sidelhorn north ridge is the coinciding lithological contact between the SWAGr and the Grimsel Zone (Moir et al. 2013). Structurally, the Grimsel Zone is relatively anisotropic in comparison to the SWAGr, which provides a complex network of reactivation possibilities.

Inter-slip mineralisation and consequent fault-healing can also force progressive increases in damage zone extent over sequential deformation stages (Finzi et al. 2011; Soden et al. 2014). Fault-surface permeability and mineralising fluid flow is clearly enhanced around the fault linkages, facilitating relatively efficient inter-slip healing relative to the restricted damage zone along the central section. Following initial brittle faulting along the GBF, this healing mineralisation would have cemented the weak, freshly broken breccias and damage zone into the indurated fault zone that is currently outcropping. The induration of the GBF in comparison to its host rocks can be directly observed from morphologically prominent, cemented breccias around the Sidelhorn linkage zone. Following mineralisation, subsequent deformation would then have been encouraged on the border of the cemented fault zone, further widening the damage zone in combination with linkage propagation (Soden et al. 2014). Efficient inter-slip healing by mineralisation and subsequent distributed fracturing partly explains the GBF's contrasting architecture to other nearby brittle faults; which are characterised by discrete fault gouges and a paucity of significant hydrothermal influence (Keusen et al. 1989; Kralik et al. 1992; Wehrens 2015).

5.3 Fluid flow

Hydrothermal activity, both recent and during formation, differentiates the GBF from the multitude of other late brittle structures in the Aar massif (Ziegler et al. 2014; Wehrens 2015). Mineralisation in and around the breccias records paleo-fluid flow extent and periodicity, while the currently discharging springs at Gletsch and in the Transitgas tunnel provide a window into the presently active system. A focused fluid pathway is required to channel fluids to the topographic high at Grimsel Pass. Such a pathway must consist of a permeable zone, a fluid conduit, encapsulated in 3D (except in the flow direction) by lower permeability, i.e., fluid sealing structures. Our results suggest viable, field-demonstrated solutions for both of these components.

5.3.1 Paleo-fluid pathways

Epithermal-style mineralisation at Grimsel Pass is clearly limited to within 150 m of the GBF (Fig. 3). The

mineralisation is associated with brittle deformation features along the fault, enhancing its permeability relative to the host rock, and tapping a fluid pathway 4 ± 1 km long from reservoir to discharge point. At the map scale, this fluid pathway is split into two first order up-flow zones (the Sidelhorn linkage and the Grimsel-Pass Gletsch zone) by the central section, where mineralising flow was closely restricted to the fault core (Fig. 3). Similar along-strike alternation between fault core and damage zone dominated permeability has been reported elsewhere (Laubach et al. 2014). At Grimsel Pass, the local geometry of pre-existing SZs resulted in major fault linkages at the north ridge of the Sidelhorn. The releasing fault bends along this particular linkage (Fig. 8) favour dilatant fracturing and fluid access (Sibson 1996). This association between fault bends and fluid flow has been well documented elsewhere (Sibson 1996; Perello et al. 2001; Moir et al. 2013; Micklithwaite et al. 2015).

Though faults can be simplified as planar structures, channelised, 'pipe-like' fluid flow along faults is supported by experimental (Lunn et al. 2008), numerical modelling (Brown and Bruhn 1998; Jourde et al. 2002; Matthäi and Belayneh 2004; Odling et al. 2004) as well as field evidence (Annunziatellis et al. 2008; Barton et al. 1995; Dockrill and Shipton 2010; Burnside et al. 2013). Our data support these concepts, and the GBF's mineralisation record demonstrates their relevance from the kilometre to millimetre scale.

The Sidelhorn linkage zone is the widest and most strongly mineralised zone along the GBF, and by inference, acted as a major fluid pathway. GSZs 1 and 2 are remarkably parallel with similar dip orientations. The resulting 3D projections of these SZs suggest that a fault linkage may persist to >1 km depth (Fig. 9), as a sub-vertically oriented 'pipe'-like fluid pathway (Fig. 10), while the linkage between GSZ 2 and 3 tapers away within 1 km of the surface.

Along the Grimsel Pass-Gletsch Zone, mineralisation is less intense than at the Sidelhorn linkage zone, as illustrated by the reduced areal extent of 'mineralised outcrop' and lower frequency of secondary structures (Fig. 3). Between Grimsel Pass and Gletsch, major fault linkages do not exist. Rather, the mineralisation is associated with discrete secondary faults and joints in a particularly wide damage zone, which fades out away from the fault. Fault architecture along the Grimsel Pass-Gletsch Zone approaches the classic distributed-conduit model of Caine et al. (1996), and this constitutes a second, eastern up-flow zone (Fig. 10). The reason for the fluid-accessible damage zone widening from W to E, particularly in comparison to the central section, is not clear from our data. Gradual contextual changes that develop from W-E in correlation with the Grimsel-Pass-Gletsch up-flow zone may be responsible.

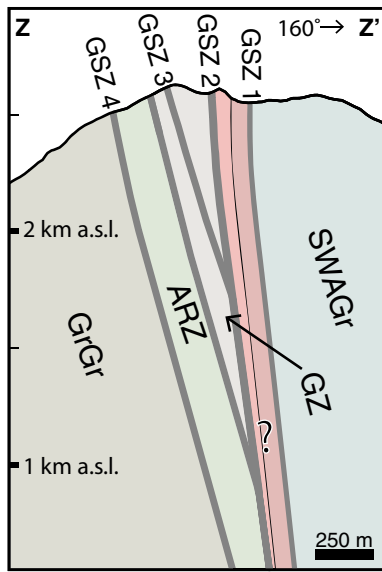


Fig. 9 Cross section across the Sidelhorn Linkage Zone. Marked from Z to Z' on Fig. 3 with the same symbology. The major SZs are projected (after Baumberger 2015) to 2 km depth below surface, based on the surface trace over the steep topography, field-collected dip data, and the Transitgas tunnel intersection

The GBF approaches the major Southern Boundary SZ (Fig. 3: SB SZ) separating the SWAGr and Ausserberg-Avat Zone. Stresses may have been locally perturbed with increasing proximity to the Southern Boundary SZ if faulting was active along it concurrently with slip along the GBF (Hardebeck and Hauksson 1999). Moreover, the mechanical contrast between the SWAGr and amphibolites in the Ausserberg-Avat Zone may exacerbate this potential stress perturbation (Yamashita 2009; Hirano and Yamashita 2011). The second E-W progression is a gradual taper of the SWAGr and its SZs, with a qualitatively observed slight increase in schistosity and SZ frequency. An increasingly schistose fabric from west to east should reduce background permeability (Stober and Bucher 2007), hindering pore-fluid pressure equilibration and consequently encouraging brittle fracturing (Secor 1965). Furthermore, an abundance of pre-existing structures provided increased opportunity for distributed brittle reactivation.

At the outcrop scale, further fluid pathway heterogeneity is observed. Mineralisation, and by inference, fluid access is focused within metre to decametre scale fingers, lobes and patches controlled by localised fault zone features. These features may result from initial, pre-mineralisation controls or may have developed during the slip history of the GBF (see also: Soden et al. 2014). The mapped ‘mineralised outcrop’ shapes (Fig. 3) are somewhat influenced by outcrop availability, especially east of position D (Fig. 3). With this in mind, the accuracy of the ‘mineralised outcrop’ zone’s shape or extent deteriorates east of this point. Nevertheless, the mapped zones feature a

notably higher density of mineralised features than their surroundings, and therefore suggest metre-scale zones of focused fluid flow within the damage zone.

5.3.2 Active fluid pathways

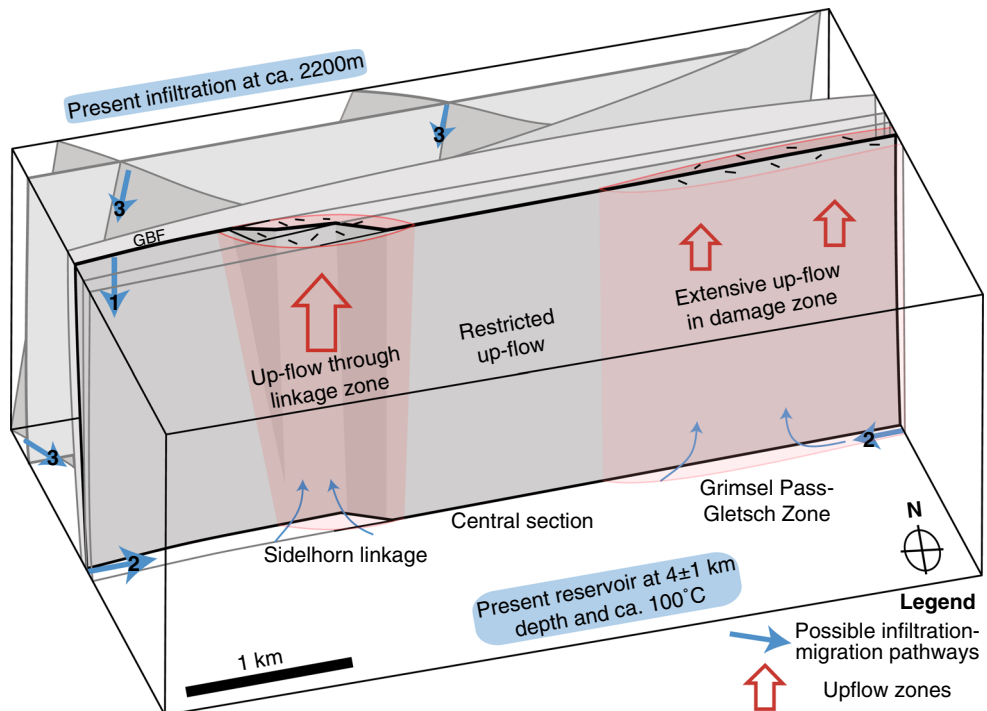
Presently discharging hydrothermal waters also provide evidence for continued channelisation of fluid pathways within the GBF system. If the tunnel inflows at 1908 m a.s.l. are effectively connected along-strike to the valley floor (0.8 km away) or the Gletsch spring (1.4 km away) at 1760 m a.s.l., waters would be unable to ascend to the tunnel (Fig. 11). This situation requires vertical sealing over 150 m, both normal to the fault and along strike between the apparently disconnected discharge points.

The sealing capabilities of mylonitic SZs are demonstrated at the Sidelhorn linkage zone (Fig. 3). East of the Sidelhorn, our mapping shows that GSZ 3 (2–5 m thickness) sharply bounds mineralisation extent and by inference, paleo-fluid access. If the mineralising fluid could have freely passed through this SZ, background fractures on the NW side should be mineralised. This sealing effect can be explained by the petrology of the mylonites: dominated by aligned phyllosilicates and with low permeability (Wehrens 2015). The major WSW-ENE striking GSZ set around Grimsel Pass is laterally extensive over tens of kilometres, steeply oriented and, at depths >1 km, appears to converge into two or three parallel SZs (Fig. 9).

It follows from this observation that GBF-parallel SZs along the Grimsel Pass-Gletsch Zone are capable of restricting fluid flow. These SZs then laterally seal the ascension paths along the GBF, channelling both the mineralising and the presently discharging fluids into the fractured damage zone, sealing the tunnel inflows from the valley floor. WSW-ENE sealing along the GBF system, between the tunnel inflows and the Gletsch spring, can be explained by along-strike differences in the damage-zone fracture network (Fig. 4), in combination with porosity occlusion by mineralisation (Fig. 7c). These sealed channels provide the hydrogeological plumbing required to bring fluids from 4 ± 1 km depth to a topographic high, purely by the hydrostatic head difference of ca. 300 m between infiltration and discharge (Fig. 11).

In the Transitgas tunnel, the 250 m wide zone of thermal fluid discharge, approximately perpendicular to the GBF plane, must be connected to deep fluid pathways (Pfeifer et al. 1992). The extent of this contemporary fluid pathway is similar in width to the ca. 250 m extent of mineralisation mapped above at the surface (Fig. 3). However, the springs described by Pfeifer et al. (1992) are offset approximately 100 m to the south. This offset cannot be explained by the generally steeply dipping local structures. The approximate correspondence in width implies that controls on Pliocene

Fig. 10 Conceptual model of the structures and fluid pathways at Grimsel Pass. The top surface is cut through the 3D model at 2700 m a.s.l. and the vertical and horizontal scales are equal. Structures south of the GBF are stripped away. Sub-vertically oriented, ‘pipe’-like up-flow zones, in the Sidelhorn Linkage Zone and Grimsel Pass-Gletsch Zone are indicated. Hydraulic constraints are annotated after Pfeifer et al. (1992) and Hofmann et al. (2004). Possible fluid infiltration and migration pathways are indicated: (1) Directly down the GBF, either side of up-flow zones. (2) Lateral migration along GBF. (3) Through the regional SZ network, including NW–SE oriented faults that may intersect the GBF and its host SZs at depth



fluid flow at Grimsel Pass are still somewhat relevant to present-day hydrothermal activity. However, the 100 m offset can be explained by two possibilities: the 3D fluid pathway is either irregularly shaped, or has evolved since the (now) surface mineralisation occurred.

Within the tunnel itself, thermal water issues from distinct points rather than continuously through the entire fracture network (Schneider 1974; Pfeifer et al. 1992; this study). These discrete inflows indicate localised flow paths within the damage zone still operate in today’s system, as the modern expression of fault-zone permeability heterogeneity recorded by ‘mineralised outcrops’ (Fig. 3).

5.3.3 Dynamic flow

Evidence for the continual evolution of fluid pathways along the GBF can be observed at the map to microstructural scale from its formation to the present. Microstructures in the fault core breccias and sequential banding of different quartz varieties records polycyclic deformation and mineralising fluids with fluctuating properties (Fig. 7c, f).

Assuming amagmatic, topographically driven circulation, dynamic fluctuations in reservoir conditions from external inputs seem unlikely in this system, and in that sense the GBF is a remarkable natural laboratory. Variation in the fluid properties can instead be explained by the periodic readjustment of the flow system by multiple successive deformation and mineralisation events: tapping deeply circulated fluids in equilibrium with microcrystalline

quartz at higher temperatures. Gradual pressure build-up in high topography would increase pore fluid pressure until fault-normal stress was overcome and slip, deformation and dilatancy occurred, draining the fluids and transitioning from over-pressured to under-pressured: naturally hydrofracturing the GBF and generating new fluid pathways (Sibson 1990). As fault-scale fluid flow system evolved with progressive deformation and mineralisation, the late, celadonitic chert mineralising fluid (Fig. 5f) was restricted to the eastern third of the fault, perhaps because of its lower topography or because fluid pathways along the central and western sections were sealed off.

Between the different studies in 1974, 1992 (Schneider 1974; Pfeifer et al. 1992) and this study in 2014, differences on the order of 10s of metres exist at the damage-zone scale between the precise locations and total extent of the thermal tunnel inflows. This evolution hints at decadal-scale temporal variation in the morphology and extent of these damage zone fluid pathways, probably as the combined result of variable surface influence and continued mineral precipitation around the tunnel (Hofmann et al. 2004).

5.3.4 Infiltration paths

It follows from the assertion of hydraulic sealing by SZs that the same features should govern the infiltration and migration of fluids into the GBF system. We postulate three possible fluid infiltration paths in Fig. 11, based on

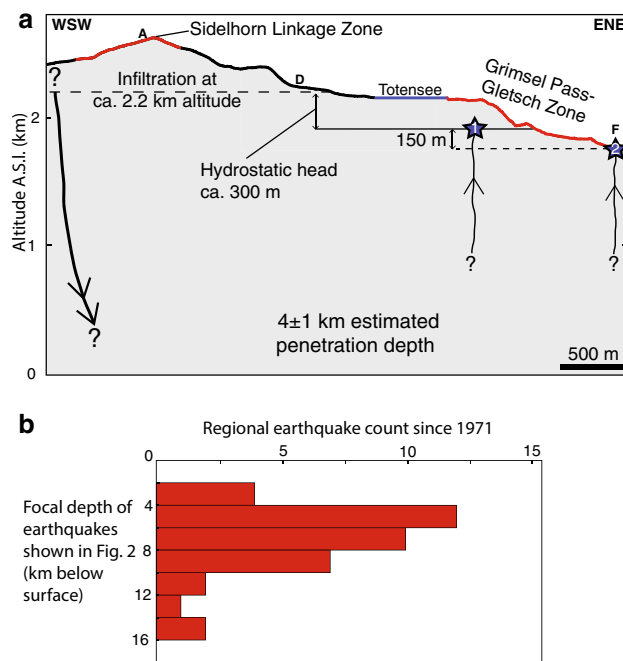


Fig. 11 **a** Hydrogeological profile along the GBF trace (points A, D, and F from Fig. 3 are marked), with (1) Transitgas Tunnel inflows, (2) Gletsch spring, and major mineralised zones (red), lakes (blue), and dashed hydrological constraints for infiltration (Pfeifer et al. 1992) and discharge. **b** The focal depths of 38 earthquakes in the area covered by Fig. 2, recorded since 1971 with magnitudes from 0.1 to 2.5, with the corresponding epicentres marked on Fig. 2 (Swiss Seismological Service 2009; Deichmann et al. 2011, 2012; Diehl et al. 2013, 2014, 2015)

previously defined hydrogeological parameters and the newly modelled structures. (1) Infiltration may be limited to the GBF or embrittled GSZs 1–3. Down-flow could occur along the central section or any along-strike fracture networks directly adjacent to the GBF, while connectivity to the reservoir depth is already demonstrated by the up-flow. The involvement of surface waters during mineralisation is suggested by notable enrichment of Mo and U in the breccias: elements more likely to be mobile in oxidising surface waters than reducing, deeply circulated waters (Hofmann et al. 2004; Greber et al. 2011). (2) The major SZ set hosting the GBF extends for 10s of km along-strike from the study area (Baumberger 2015). These SZs could channel migrating fluids from along-strike either side of the GBF. (3) Mapping by Rolland et al. (2009), Baumberger (2015) and Wehrens (2015) shows a major NW–SE oriented SZ set oblique to GSZs 1–4, as well as further SZ sets parallel to GSZs 1–4 (Fig. 3). The resulting SZ pattern pervasively dissects the entire southern part of the Aar massif (Fig. 1). Many of these NE–SW and NW–SE striking SZs were reactivated in a brittle manner, providing potential fluid pathways. Sub-thermal springs in Val d’Illiez, Valais issue 9 km from their infiltration point

(Bianchetti et al. 1992), after circulating deep enough to attain a discharge temperature of 30 °C; so fluid migration pathways of a potentially similar length to the GBF are demonstrated in the region.

The question of what drives fluid infiltration against the regional hydraulic gradient to 4 ± 1 km depth and around 100 °C (Pfeifer et al. 1992) is still open. The microstructural record of the GBF suggests a close interplay between brittle deformation, dilatancy formation and episodic fluid flow at these depths. These processes probably continue to operate today, as suggested by the longevity of what should be a self-sealing hydrothermal system (Cox et al. 2001). This inference is corroborated by recent seismic activity in the area (Fig. 1), where the focal points of low magnitude earthquakes coincide with the domains we consider for fluid infiltration (Fig. 10: 1–3), and with the deepest levels of the Grimsel hydrothermal system (Fig. 11b).

Dilatancy during fault displacement is coupled with a reduction in fault-zone pore fluid pressure that may last for tens to hundreds of years (Matthäi and Fischer 1996; Matthäi and Roberts 1997). Accordingly, recurrent slip events along regional faults, as suggested by fossil microstructures (Fig. 7f) and active seismicity (Fig. 11b), provide a mechanism for generating the transient low pressures at depth required to bring meteoric fluids below the water table. Down-flow is then maintained by what is in effect an inverted siphon (Fig. 11a): with a high volume, low permeability reservoir under hydrostatic pressure feeding into the low volume, high permeability up-flow zones along the GBF, which provide a sealed fluid pathway to discharge points below the infiltration altitude.

5.4 Potential applicability

Knowledge of fault zone architecture in crystalline basement is critical to the efficient development of certain geothermal, waste storage, CO₂ sequestration, ore, and hydrocarbon resources. Our findings are of particular relevance to geothermal energy exploration of similar systems in the Alps (e.g., Brigerbad, Leukerbad, Lavey les Bains) or in analogous crystalline basement of the Northern Alpine Foreland Basin (NAFB). We propose the Aar massif basement rocks constitute a relevant analogue to the deep geothermal target basement rocks to the north. The Grimsel Pass meta-granites and polymetamorphosed gneisses share petrological and hydrogeological similarities with the crystalline basement of the NAFB (Thury et al. 1994). Strike-slip faults and seismic activity are well documented extending into the crystalline basement of the NAFB (Deichmann 1992; Kastrup et al. 2007; Singer et al. 2014). Although the Grimsel basement experienced higher grade and intensity Alpine deformation than the NAFB basement, Variscan structures are certainly present in country rocks as

well as syn-collisional Variscan plutons (Finger et al. 1998), providing mechanical anisotropies that influenced later Alpine and neotectonic deformation (Edel et al. 2007).

Fossil hydrothermal systems in the northern continuation of the geothermally prospective basement in the Black Forest massif share some similarities with the GBF. Post-Variscan epithermal mineralisation occurred at 90–200 °C (Baatartsogt et al. 2007) and was occasionally associated with brittle fault intersections (Staude et al. 2011). Our study suggests that the characteristic deformation processes and resultant fault architectures of the GBF are inseparably connected to pre-existing structures and hydrothermal influence during deformation. Given these similarities, highly heterogeneous permeability around fault zones, as well as potentially impermeable Variscan mylonites should be expected in the NAFB basement. In this sense, the GBF is an ideal site to test our understanding of the links between deformation and hydrothermal fluid flow in the inaccessible NAFB basement at depths of 3–5 km.

6 Conclusions

Fault zone hydraulic properties are notoriously difficult to predict and interpolate (Lunn et al. 2008), and our results reinforce this uncertainty. We find that strike-slip fault-associated permeability is strongly heterogeneous in time and space. However, the data ties certain hydraulic architectures to specific structural situations.

At Grimsel Pass, we find that:

- With progressive exhumation, brittle faulting at Grimsel Pass is geometrically controlled by pre-existing mylonitic SZs formed at higher grade.
- Mylonitic SZs are capable of acting as hydraulic seals.
- Fault zone permeability structure is strongly controlled by local fault complexities, resulting in localised ‘pipe’-like structures channelising fluid flow within the fault zone.

With these points in mind, linkage zones along strike-slip faults are shown to be highly permeable features, most likely occurring in crystalline basement with a polyphase deformation history (e.g., the NAFB). For these reasons, fault linkages are prime targets for hydrothermal circulation or naturally enhanced fracture permeability: compelling alternatives to artificially stimulated permeability (Moeck 2014). At present, successful prediction of steeply dipping basement faults and their complexities in the NAFB is an obstacle to their exploitation; however, with suitable geotools (structural geology, geophysics, dilatancy modelling and select drilling) it may be possible to successfully target these zones at depth (e.g., Siler et al. 2016).

Acknowledgments Reviews from James Evans and Zoe Shipton were appreciated for improving the manuscript. We thank Beda Hofmann (Natural History Museum of Bern) for his introduction to the breccias and sample access, and also Philip Wehrens and Roland Baumberger for providing their 3D data. Transit Gas AG kindly provided tunnel access. We are grateful for constructive reviews, discussion and fieldwork with Daniel Egli, Larryn Diamond and Raphael Schneberger. This work has been completed within the Swiss Competence Center on Energy Research-Supply of Electricity (SCCER-SoE).

References

- Abrecht, J. (1994). Geologic units of the Aar massif and their pre-Alpine rock associations: a critical review : the pre-Alpine crustal evolution of the Aar-, Gotthard- and Tavetsch massifs. *Schweizerische Mineralogische und Petrographische Mitteilungen*, 74(1), 5–27.
- Allmendinger, R. (2014). Stereonet 9. <http://www.geo.cornell.edu/geology/faculty/RWA/programs/stereonet.html>. Accessed 14 July 2015.
- Annunziatellis, A., Beaubien, S., Bigi, S., Ciotoli, G., Coltellà, M., & Lombardi, S. (2008). Gas migration along fault systems and through the vadose zone in the Latera caldera (central Italy): implications for CO₂ geological storage. *International Journal of Greenhouse Gas Control*, 2(3), 353–372.
- Baatartsogt, B., Schwinn, G., Wagner, T., Taubald, H., Beitter, T., & Markl, G. (2007). Contrasting paleofluid systems in the continental basement: a fluid inclusion and stable isotope study of hydrothermal vein mineralization, Schwarzwald district, Germany. *Geofluids*, 7(2), 123–147.
- Baietto, A., Perello, P., Cadoppi, P., & Martinotti, G. (2009). Alpine tectonic evolution and thermal water circulations of the Argentera Massif (South-Western Alps). *Swiss Journal of Geosciences*, 102(2), 223–245.
- Barton, C. A., Zoback, M. D., & Moos, D. (1995). Fluid flow along potentially active faults in crystalline rock. *Geology*, 23(8), 683–686.
- Baumberger, R. (2015). Quantification of lineaments: link between internal 3D structure and surface evolution of the Hasli valley (Aar massif, Central alps, Switzerland). *PhD dissertation*. Universität Bern.
- Bergemann, C., Gnos, E., Berger, A., Whitehouse, M., Pettke, T., & Janots, E. (2014). Shear zone activity of the Grimsel area (Aar-massif): Th–Pb data in hydrothermal cleft monazite. In *Abstracts of Swiss Geoscience Meeting*.
- Bianchetti, G., Roth, P., Vuataz, F., & Vergain, J. (1992). Deep groundwater circulation in the Alps: relations between water infiltration, induced seismicity and thermal springs. The case of Val d'Illiez, Valais, Switzerland. *Eclogae Geologicae Helvetiae*, 85(2), 291–305.
- Bistacchi, A., Massironi, M., Menegon, L., Bolognesi, F., & Donghi, V. (2012). On the nucleation of non-Andersonian faults along phyllosilicate-rich mylonite belts. *Geological Society, London, Special Publications*, 367(1), 185–199.
- Bodmer, P. (1982). Geothermal Map of Switzerland. *Schweiz. geophys. Komm.* Bern: Kümmerly und Frey.
- Brown, S. R., & Bruhn, R. L. (1998). Fluid permeability of deformable fracture networks. *Journal of Geophysical Research: Solid Earth*, 103(2), 2489–2500.
- Burnside, N. M., Shipton, Z. K., Dockrill, B., & Ellam, R. M. (2013). Man-made versus natural CO₂ leakage: a 400 k.y. History of an analogue for engineered geological storage of CO₂. *Geology*, 41(4), 471–474.

- Byerlee, J. (1978). Friction of rocks. *Pure and Applied Geophysics*, 116(4–5), 615–626.
- Caine, J. S., Evans, J. P., & Forster, C. B. (1996). Fault zone architecture and permeability structure. *Geology*, 24(11), 1025–1028.
- Campani, M., Mancktelow, N., Seward, D., Rolland, Y., Müller, W., & Guerra, I. (2010). Geochronological evidence for continuous exhumation through the ductile-brittle transition along a crustal-scale low-angle normal fault: Simplon Fault Zone, central Alps. *Tectonics*, 29(3), TC3002.
- Challandes, N., Marquer, D., & Villa, I. M. (2008). P-T-t modelling, fluid circulation, and 39Ar-40Ar and Rb-Sr mica ages in the Aar massif shear zones (Swiss Alps). *Swiss Journal of Geosciences*, 101(2), 269–288.
- Chester, F. M., & Logan, J. M. (1986). Implications for mechanical properties of brittle faults from observations of the Punchbowl fault zone, California. *Pure and Applied Geophysics*, 124(1–2), 79–106.
- Cox, S. F., Knackstedt, M., & Braun, J. (2001). Principles of structural control on permeability and fluid flow in hydrothermal systems. *Reviews in Economic Geology*, 14, 1–24.
- Crider, J. G. (2015). The initiation of brittle faults in crystalline rock. *Journal of Structural Geology*, 77, 159–174.
- Deichmann, N. (1992). Structural and rheological implications of lower-crustal earthquakes below northern Switzerland. *Physics of the Earth and Planetary Interiors*, 69(3–4), 270–280.
- Deichmann, N., Clinton, J., Husen, S., Edwards, B., Haslinger, F., Fäh, D., et al. (2011). Earthquakes in Switzerland and surrounding regions during 2010. *Swiss Journal of Geosciences*, 104(3), 537–547.
- Deichmann, N., Clinton, J., Husen, S., Edwards, B., Haslinger, F., Fäh, D., et al. (2012). Earthquakes in Switzerland and surrounding regions during 2011. *Swiss Journal of Geosciences*, 105(3), 463–476.
- Diehl, T., Clinton, J., Kraft, T., Husen, S., Plenkens, K., Guilhelm, A., et al. (2014). Earthquakes in Switzerland and surrounding regions during 2013. *Swiss Journal of Geosciences*, 107(2–3), 359–375.
- Diehl, T., Deichmann, N., Clinton, J., Husen, S., Kraft, T., Plenkens, K., et al. (2013). Earthquakes in Switzerland and surrounding regions during 2012. *Swiss Journal of Geosciences*, 106(3), 543–558.
- Diehl, T., Deichmann, N., Clinton, J., Kästli, P., Cauzzi, C., Kraft, T., et al. (2015). Earthquakes in Switzerland and surrounding regions during 2014. *Swiss Journal of Geosciences*, 108(2–3), 425–443.
- Dockrill, B., & Shipton, Z. K. (2010). Structural controls on leakage from a natural CO₂ geologic storage site: Central Utah, USA. *Journal of Structural Geology*, 32(11), 1768–1782.
- Edel, J. B., Schulmann, K., & Rotstein, Y. (2007). The Variscan tectonic inheritance of the Upper Rhine Graben: evidence of reactivations in the Lias, Late Eocene-Oligocene up to the recent. *International Journal of Earth Sciences*, 96(2), 305–325.
- Eichhubl, P., Davatzes, N. C., & Becker, S. P. (2009). Structural and diagenetic control of fluid migration and cementation along the Moab fault, Utah. *AAPG Bulletin*, 93(5), 653–681.
- Evans, J. P., Forster, C. B., & Goddard, J. V. (1997). Permeability of fault-related rocks, and implications for hydraulic structure of fault zones. *Journal of Structural Geology*, 19(11), 1393–1404.
- Faulkner, D. R., Jackson, C. A. L., Lunn, R. J., Schlische, R. W., Shipton, Z. K., Wibberley, C. A. J., & Withjack, M. O. (2010). A review of recent developments concerning the structure, mechanics and fluid flow properties of fault zones. *Journal of Structural Geology*, 32(11), 1557–1575.
- Fernández, O. (2005). Obtaining a best fitting plane through 3D georeferenced data. *Journal of Structural Geology*, 27(5), 855–858.
- Finger, F., Roberts, M. P., Haunschmid, B., Schermaier, A., & Steyer, H. P. (1998). Variscan granitoids of central Europe: their typology, potential sources and tectonothermal relations. *Mineralogy and Petrology*, 61(1–4), 67–96.
- Finzi, Y., Hearn, E. H., Lyakhovsky, V., & Gross, L. (2011). Fault-zone healing effectiveness and the structural evolution of strike-slip fault systems. *Geophysical Journal International*, 186(3), 963–970.
- Fourcade, S., Marquer, D., & Javoy, M. (1989). ¹⁸O/¹⁶O variations and fluid circulation in a deep shear zone: the case of the Alpine ultramylonites from the Aar massif (Central Alps, Switzerland). *Chemical Geology*, 77(2), 119–131.
- Glötzbach, C., Reinecker, J., Danišík, M., Rahn, M., Frisch, W., & Spiegel, C. (2010). Thermal history of the central Gotthard and Aar massifs, European Alps: evidence for steady state, long-term exhumation. *Journal of Geophysical Research: Earth Surface*, 115(3), F03017.
- Greber, N. D., Hofmann, B. A., Voegelin, A. R., Villa, I. M., & Nägler, T. F. (2011). Mo isotope composition in Mo-rich high- and low-T hydrothermal systems from the Swiss Alps. *Geochimica et Cosmochimica Acta*, 75(21), 6600–6609.
- Hardebeck, J. L., & Hauksson, E. (1999). Role of fluids in faulting inferred from stress field signatures. *Science*, 285(5425), 236–239.
- Hirano, S., & Yamashita, T. (2011). Analysis of the static stress field around faults lying along and intersecting a bimaterial interface. *Geophysical Journal International*, 187(3), 1460–1478.
- Hofmann, B. A., Helfer, M., Diamond, L. W., Villa, I. M., Frei, R., & Eikenberg, J. (2004). Topography-driven hydrothermal breccia mineralization of Pliocene age at Grimsel Pass, Aar massif, Central Swiss Alps. *Schweizerische Mineralogische und Petrographische Mitteilungen*, 84(3), 271–302.
- Hubbard, M., & Mancktelow, N. S. (1992). Lateral displacement during Neogene convergence in the western and central Alps. *Geology*, 20(10), 943–946.
- Janssen, C., Wagner, F. C., Zang, A., & Dresen, G. (2001). Fracture process zone in granite: a microstructural analysis. *International Journal of Earth Sciences*, 90(1), 46–59.
- Jourde, H., Flodin, E. A., Aydin, A., Durlofsky, L. J., & Wen, X. H. (2002). Computing permeability of fault zones in eolian sandstone from outcrop measurements. *AAPG Bulletin*, 86(7), 1187–1200.
- Kamb, W. B. (1959). Ice petrofabric observations from Blue Glacier, Washington, in relation to theory and experiment. *Journal of Geophysical Research*, 64(11), 1891.
- Kastrup, U., Deichmann, N., Fröhlich, A., & Giardini, D. (2007). Evidence for an active fault below the northwestern Alpine foreland of Switzerland. *Geophysical Journal International*, 169(3), 1273–1288.
- Keusen, H. R., Ganguin, J., Schuler, P., & Buletti, M. (1989). *Nagra Technical Report 87-14*. E. Bern.
- Kirkpatrick, J. D., Shipton, Z. K., Evans, J. P., Micklethwaite, S., Lim, S. J., & McKillop, P. (2008). Strike-slip fault terminations at seismogenic depths: the structure and kinematics of the Glacier Lakes fault, Sierra Nevada United States. *Journal of Geophysical Research*, 113(B4), B04304.
- Kralik, M., Clauer, N., Holsteiner, R., Huemer, H., & Kappel, R. H. (1992). Recurrent fault activity in the Gimsel Test Site (GTS, Switzerland); revealed by Rb-Sr, K-Ar and tritium isotope techniques. *Journal of the Geological Society of London*, 149(2), 293–301.
- Kranz, R. L. (1983). Microcracks in rocks: a review. *Tectonophysics*, 100(1–3), 449–480.
- Laubach, S. E., Eichhubl, P., Hargrove, P., Ellis, M. A., & Hooker, J. N. (2014). Fault core and damage zone fracture attributes vary along strike owing to interaction of fracture growth, quartz

- accumulation, and differing sandstone composition. *Journal of Structural Geology*, 68, 207–226.
- Lunn, R. J., Shipton, Z., & Bright, A. (2008a). How can we improve estimates of bulk fault zone hydraulic properties? *Geological Society, London, Special Publications*, 299, 231–237.
- Lunn, R. J., Willson, J. P., Shipton, Z. K., & Moir, H. (2008b). Simulating brittle fault growth from linkage of preexisting structures. *Journal of Geophysical Research: Solid Earth*, 113(B7), B07403.
- Matthäi, S. K., & Belayneh, M. (2004). Fluid flow partitioning between fractures and a permeable rock matrix. *Geophysical Research Letters*, 31(7), L07602.
- Matthäi, S. K., & Fischer, G. (1996). Quantitative modeling of fault-fluid-discharge and fault-dilation-induced fluid-pressure variations in the seismogenic zone. *Geology*, 24(2), 183–186.
- Matthäi, S. K., & Roberts, S. G. (1997). Transient versus continuous fluid flow in seismically active faults: An investigation by electric analogue and numerical modelling. In B. Jamtveit & B. W. D. Yardley (Eds.), *Fluid Flow and Transport in Rocks: Mechanisms and effects* (pp. 263–295). Dordrecht: Springer Netherlands.
- Mauldon, M., Dunne, W. M., & Rohrbaugh, M. B. (2001). Circular scanlines and circular windows: new tools for characterizing the geometry of fracture traces. *Journal of Structural Geology*, 23(2–3), 247–258.
- Maurer, H. R., Burkhard, M., Deichmann, N., & Green, A. G. (1997). Active tectonism in the central Alps: contrasting stress regimes north and south of the Rhone Valley. *Terra Nova*, 9, 91–94.
- Micklethwaite, S., Ford, A., Witt, W., & Sheldon, H. A. (2015). The where and how of faults, fluids and permeability—insights from fault stepovers, scaling properties and gold mineralisation. *Geofluids*, 15(1–2), 240–251.
- Mitchell, T. M., & Faulkner, D. R. (2009). The nature and origin of off-fault damage surrounding strike-slip fault zones with a wide range of displacements: a field study from the Atacama fault system, northern Chile. *Journal of Structural Geology*, 31(8), 802–816.
- Moeck, I. S. (2014). Catalog of geothermal play types based on geologic controls. *Renewable and Sustainable Energy Reviews*, 37, 867–882.
- Moir, H., Lunn, R. J., Micklethwaite, S., & Shipton, Z. K. (2013). Distant off-fault damage and gold mineralization: the impact of rock heterogeneity. *Tectonophysics*, 608, 461–467.
- Morey, G., Fournier, R., & Rowe, J. (1962). The solubility of quartz in water in the temperature interval from 25 to 300 °C. *Geochimica et Cosmochimica Acta*, 26(10), 1029–1043.
- Morrow, C. A., & Lockner, D. A. (1994). Permeability differences between surface-derived and deep drillhole core samples. *Geophysical Research Letters*, 21(19), 2151–2154.
- Niggli, C. R. (1965). Petrographie und Petrogenesis der Migmatite und Gneise im südlichen Aarmassiv zwischen Obergesteln und Furkapass. *PhD Dissertation*. Universität Bern.
- Oberhänsli, R., Schenker, F., & Mercolli, I. (1988). Indications of Variscan nappe tectonics in the Aar massif. *Schweizerische Mineralogische und Petrographische Mitteilungen*, 68(3), 509–520.
- Odling, N. E., Harris, S. D., & Knipe, R. J. (2004). Permeability scaling properties of fault damage zones in siliciclastic rocks. *Journal of Structural Geology*, 26(9), 1727–1747.
- Perello, P., Marini, L., Martinotti, G., & Hunziker, J. C. (2001). The thermal circuits of the Argentera Massif (western alps, Italy): an example of low-enthalpy geothermal resources controlled by Neogene alpine tectonics. *Eclogae Geologicae Helvetiae*, 94(1), 75–94.
- Petit, J. P. (1987). Criteria for the sense of movement on fault surfaces in brittle rocks. *Journal of Structural Geology*, 9(5–6), 597–608.
- Pfeifer, H. R., Sanchez, A., & Deguelde C. (1992). Thermal springs in granitic rocks from the Grimsel Pass (Swiss Alps); the late stage of a hydrothermal system related to Alpine Orogeny. In *Water Rock Interaction* (Vol. 7, pp. 1327–1331). Rotterdam: International Association of Geochemistry and Cosmochemistry and Alberta Research Council, Sub-Group on Water-Rock Interaction Edmonton, AB, International.
- Pleuger, J., Mancktelow, N., Zwingmann, H., & Manser, M. (2012). K-Ar dating of synkinematic clay gouges from Neoalpine faults of the Central, Western and Eastern Alps. *Tectonophysics*, 550–553, 1–16.
- Rawling, G. C., Goodwin, L. B., & Wilson, J. L. (2001). Internal architecture, permeability structure, and hydrologic significance of contrasting fault-zone types. *Geology*, 29(1), 43–46.
- Rimstidt, J. D. (1997). Quartz solubility at low temperatures. *Geochimica et Cosmochimica Acta*, 61(13), 2553–2558.
- Rolland, Y., Cox, S. F., & Corsini, M. (2009). Constraining deformation stages in brittle-ductile shear zones from combined field mapping and 40Ar/39Ar dating; the structural evolution of the Grimsel Pass area (Aar massif, Swiss Alps). *Journal of Structural Geology*, 31(11), 1377–1394.
- Rowe, C. D., & Griffith, W. A. (2015). Do faults preserve a record of seismic slip: a second opinion. *Journal of Structural Geology*, 78, 1–26.
- Rybáček, L. (1995). Thermal waters in deep Alpine tunnels. *Geothermics*, 24(5–6), 631–637.
- Savage, H. M., & Brodsky, E. E. (2011). Collateral damage: evolution with displacement of fracture distribution and secondary fault strands in fault damage zones. *Journal of Geophysical Research: Solid Earth*, 116(3), B03405.
- Schaltegger, U. (1990). Post-magmatic resetting of Rb-Sr whole rock ages—a study in the Central Aar Granite (Central Alps, Switzerland). *Geologische Rundschau*, 79(3), 709–724.
- Schaltegger, U. (1993). The evolution of the polymetamorphic basement in the Central Alps unravelled by precise U-Pb zircon dating. *Contributions to Mineralogy and Petrology*, 113(4), 466–478.
- Schaltegger, U., Abrecht, J., & Corfu, F. (2003). The Ordovician orogeny in the Alpine basement: constraints from geochronology and geochemistry in the Aar massif (Central Alps). *Schweizerische Mineralogische und Petrographische Mitteilungen*, 83(2), 183–195.
- Schaltegger, U., & Corfu, F. (1992). The age and source of late Hercynian magmatism in the central Alps: evidence from precise U-Pb ages and initial Hf isotopes. *Contributions to Mineralogy and Petrology*, 111(3), 329–344.
- Schneider, T. R. (1974). *Geologische Stollenaufnahmen Transitgas AG: Unterstock-, Urweid-, Gstellar-, Grimsel- und Obergesteln-Stollen*. Zürich: Elektro-Watt Ingenieurunternehmung AG.
- Schulz, S. E., & Evans, J. P. (2000). Mesoscopic structure of the Punchbowl Fault, Southern California and the geologic and geophysical structure of active strike-slip faults. *Journal of Structural Geology*, 22(7), 913–930.
- Secor, D. T. (1965). Role of fluid pressure in jointing. *American Journal of Science*, 263(8), 633–646.
- Shipton, Z. K., & Cowie, P. A. (2001). Damage zone and slip-surface evolution over μm to km scales in high-porosity Navajo sandstone, Utah. *Journal of Structural Geology*, 23(12), 1825–1844.
- Shipton, Z. K., Evans, J. P., & Thompson, L. B. (2005). The Geometry and thickness of deformation-band fault core and its influence on sealing characteristics of deformation-band fault zones. *AAPG Memoir*, 85, 181–195.
- Sibson, R. H. (1985). *Stopping of earthquake ruptures at dilatational fault jogs*. Heidelberg: Nature.

- Sibson, R. H. (1986). Brecciation processes in fault zones: inferences from earthquake rupturing. *Pure and Applied Geophysics*, 124(1–2), 159–175.
- Sibson, R. H. (1990). Conditions for fault-valve behaviour. *Geological Society, London, Special Publications*, 54(1), 15–28.
- Sibson, R. H. (1996). Structural permeability of fluid-driven fault-fracture meshes. *Journal of Structural Geology*, 18(8), 1031–1042.
- Siler, D. L., Faulds, J. E., Mayhew, B., & McNamara, D. D. (2016). Analysis of the favorability for geothermal fluid flow in 3D: astor Pass geothermal prospect, Great Basin, northwestern Nevada, USA. *Geothermics*, 60, 1–12.
- Soden, A. M., Shipton, Z. K., Lunn, R. J., Pytharouli, S. I., Kirkpatrick, J. D., Do Nascimento, A. F., & Bezerra, F. H. R. (2014). Brittle structures focused on subtle crustal heterogeneities: implications for flow in fractured rocks. *Journal of the Geological Society*, 171(4), 509–524.
- Singer, J., Diehl, T., Husen, S., Kissling, E., & Duretz, T. (2014). Alpine lithosphere slab rollback causing lower crustal seismicity in northern foreland. *Earth and Planetary Science Letters*, 397, 42–56.
- Sonney, R., & Vuataz, F. D. (2008). Properties of geothermal fluids in Switzerland: a new interactive database. *Geothermics*, 37(5), 496–509.
- Stalder, H. A. (1964). Petrographische und mineralogische Untersuchungen im Grimselgebiet (Mittleres Aarmassiv). *Schweizerische Mineralogische und Petrographische Mitteilungen*, 44(1), 188–384.
- Staude, S., Werner, W., Mordhorst, T., Wemmer, K., Jacob, D. E., & Markl, G. (2011). Multi-stage Ag–Bi–Co–Ni–U and Cu–Bi vein mineralization at Wittichen, Schwarzwald, SW Germany: geological setting, ore mineralogy, and fluid evolution. *Mineralium Deposita*, 47(3), 251–276.
- Steck, A. (1966). Petrographische und tektonische Untersuchungen am zentralen Aaregranit und seinen altkristallinen Huellgestein im westlichen Aarmassiv im Gebiet Belalp-Grisighorn. *Beiträge zur die Geologischen Karte der Schweiz*, 130, 96.
- Steck, A. (1968). Die alpinischen Strukturen in den zentralen Aargraniten des westlichen Aarmassivs. *Eclogae Geologicae Helvetiae*, 61, 19–48.
- Steck, A. (1984). Structures et déformations tertiaires dans les Alpes Centrales (transversale Aar-Simplon-Ossola). *Eclogae Geologicae Helvetiae*, 77, 55–100.
- Stober, I., & Bucher, K. (2007). Hydraulic properties of the crystalline basement. *Hydrogeology Journal*, 15(2), 213–224.
- Swiss Seismological Service. (2009). Earthquake Catalog of Switzerland 2009. www.seismo.ethz.ch/prod/catalog/index. Accessed 1 Mar 2015.
- Terzaghi, R. D. (1965). Sources of error in joint surveys. *Géotechnique*, 15(3), 287–304.
- Thury, M., Gautschi, A., Mazurek, M., Müller, W. H., Naef, H., Pearson, F. J., et al. (1994). *Nagra Technical Report 93-01*. Wettingen.
- Tripp, G. I., & Vearncombe, J. R. (2004). Fault/fracture density and mineralization: a contouring method for targeting in gold exploration. *Journal of Structural Geology*, 26(6–7), 1087–1108.
- Vermilye, J. M., & Scholz, C. H. (1998). The process zone: a microstructural view of fault growth. *Journal of Geophysical Research*, 103(B6), 12223–12237.
- Vernon, A. J., Van Der Beek, P. A., Sinclair, H. D., Persano, C., Foeken, J., & Stuart, F. M. (2009). Variable late Neogene exhumation of the central European Alps: low-temperature thermochronology from the Aar massif, Switzerland, and the Lepontine Dome, Italy. *Tectonics*, 28, 1–21.
- Vuataz, F. (1982). *Hydrogéologie, géochimie et géothermie des eaux thermales de Suisse et des régions alpines limitrophes. Matériaux Géologie Suisse, série Hydrologie* (29th ed.). Bern: Kümmerly und Frey.
- Walker, R. J., Holdsworth, R. E., Armitage, P. J., & Faulkner, D. R. (2012). Fault zone permeability structure evolution in basalts. *Geology*, 41(1), 59–62.
- Wehrens, P. (2015). *Structural evolution of the Aar massif (Haslital transect): Implications for mid-crustal deformation*. Bern: Universität Bern.
- Woodcock, N. H. (1977). Specification of fabric shapes using an eigenvalue method. *Bulletin of the Geological Society of America*, 88(9), 1231–1236.
- Yamashita, T. (2009). Rupture dynamics on bimaterial faults and nonlinear off-fault damage. *International Geophysics*, 94(C), 187–215.
- Zangerl, C., Loew, S., & Eberhardt, E. (2006). Structure, geometry and formation of brittle discontinuities in anisotropic crystalline rocks of the Central Gotthard Massif, Switzerland. *Eclogae Geologicae Helvetiae*, 99(2), 271–290.
- Ziegler, M., Loew, S., & Bahat, D. (2014). Growth of exfoliation joints and near-surface stress orientations inferred from fractographic markings observed in the upper Aar valley (Swiss Alps). *Tectonophysics*, 626(1), 1–20.